Response to

Comments on "Theoretical investigation of mixing in warm clouds – Part 2: homogeneous mixing"

We are grateful for valuable comments and remarks.

© I have read the revised version of part 3 and in general I think it is ready for publication after some relatively small corrections listed below. There is clearer connection between the three parts and better physical interpretation of the results.

® Thank you.

©1. Change the legend text RH0 to RHm) in Fig. 3,8-13 to make consistent with the text.

® We replaced RH_{m0} by RH_0 across the text of paper and figure captures

©2. page 12, line 262: it is stated that "The deviation increases with an increase in parameter..." Should it be " The deviation increases with a decrease in parameter..."?

® Corrected

©3. page 15, line 322: it is stated that "...with decreasing u and increasing R"? which is not consistent with the text in figure 6b. Should it be "...with decreasing q and increasing R"?

® Corrected for "...with decreasing q_1 and increasing RH_2"

©4. I like the name of R as "potential evaporation parameter" which is defined in Part 3. It might also be good to define and explain it in Part 2.

® We added the following sentences (lines 295-299) "This parameter can be referred to as a potential evaporation parameter (PEP). The PEP is proportional to the ratio of the amount of water vapour that should evaporate in order to saturate the initially droplet-free volume (that is determined by S_2) to the initial available liquid water q_1 in the cloud volume in case of equal initial volumes $V_1 = V_2$".

Theoretical investigation of mixing in warm clouds. Part 2: Homogeneous mixing

M. Pinsky(1), A. Khain(1), A. Korolev(2) and L. Magaritz-Ronen (1)

(1) Department of Atmospheric Sciences, The Hebrew University of Jerusalem, Israel

(2) Environment Canada, Cloud Physics and Severe Weather Section, Toronto, Canada

Submitted to the Atmos. Chem. Phys.

revision (April, 2016)

second revision (May 2016)

Communicating author: Alexander Khain, The Hebrew University of Jerusalem,

alexander.khain@mail.huji.ac.il

Abstract

Evolution of monodisperse and polydisperse droplet size distributions (DSD) during homogeneous mixing is analyzed. Time-dependent universal analytical expressions for supersaturation and liquid water content are derived. For an initial monodisperse DSD, these quantities are shown to depend on a sole non-dimensional parameter. The evolution of moments and moment-related functions in the course of homogeneous evaporation of polydisperse DSD is analyzed using a parcel model.

It is shown that the classic conceptual scheme, according to which homogeneous mixing leads to a decrease in droplet mass at constant droplet concentration, is valid only in cases of monodisperse or initially very narrow polydisperse DSD. In cases of wide polydisperse DSD, mixing and successive evaporation lead to a decrease of both mass and concentration, so the characteristic droplet sizes remain nearly constant. As this feature is typically associated with inhomogeneous mixing, we conclude that in cases of an initially wide DSD at cloud top, homogeneous mixing is nearly indistinguishable from inhomogeneous mixing.

Key words: *turbulent mixing, homogeneous mixing, mono-and polydisperse droplet size distributions*

1. Introduction

Turbulent mixing at cloud edges and cloud tops accompanied by phase transitions has been the focus of numerous studies, beginning with the pioneering works of Baker and Latham (1979), Baker et al. (1980), Blyth et al. (1980) and Baker and Latham (1982). Laboratory experiments by Latham and Reed (1977) showed that after mixing with sub-saturated air some droplets completely evaporate while others remain unchanged. This finding gave rise to the concept of two types of turbulent mixing: homogeneous and inhomogeneous. A recent description of the classical concepts of homogeneous and inhomogeneous mixing can be found in study by Korolev et al. (2016), hereafter referred to as Pt1.

Figure 1 presents a conceptual scheme of homogeneous mixing between saturated cloud volume V_1 containing droplets and sub-saturated droplet-free volume V_2 (Fig. 1a) in case of initially monodisperse droplet size distribution (DSD). This scheme is the base of further analysis. According to the concept of homogeneous mixing, the air within the volumes mixes at a rate much higher than the characteristic rate of droplet evaporation. So, the fields of temperature and humidity (and, therefore, the fields of the relative humidity and supersaturation) are rapidly homogenized throughout the entire volume, and all the droplets experience the same supersaturation (Fig. 1b). At the end of the first stage, the droplet concentration decreases due to dilution down to $N_{m0} = N_1 \frac{V_1}{V_1 + V_2}$, where N_1 is the initial droplet concentration in the cloud volume. At the second stage (Fig. 1c), droplets change supersaturation and temperature through their evaporation. There are two possible scenarios for the final equilibrium states. In the first one, illustrated in Fig. 1c, droplets continue evaporating until they saturate the environment. The size of all droplets decreases, but they evaporate only partially, so the droplet concentration N_{m0} remains unchanged. In the second scenario, when the initially droplet-free volume is very dry,

106 the droplets penetrated from cloud volume evaporate completely. In case of polydisperse initial
107 DSD, both partial and complete evaporation of droplets determine the final DSD.

108 In contrast to homogeneous mixing, spatial homogenization during *inhomogeneous* mixing is
109 a relatively slow process. According to the concept of extremely inhomogeneous mixing, some
110 droplets are transported by the turbulent eddies into the dry environment and experience
111 complete evaporation, whereas other droplets remain unchanged. As in the case of homogeneous
112 mixing, the process of droplet evaporation continues until either the environment is saturated or
113 all the droplets evaporate. According to the classical concept, during extremely inhomogeneous
114 mixing the shape of DSD is conserved, however, the total droplet concentration decreases (see
115 review by Devenish et al., 2012 and Pt 1).

116 The classical concepts analyze only the final equilibrium states which are based on the mass
117 conservation consideration. Strictly speaking, the size distributions in the final states, assumed in
118 the classical concepts, are hypothetical and cannot be reached. This is because the classic
119 concepts do not take into account the mixing-induced DSD broadening. Detailed simulation of
120 time evolution of DSD and other microphysical parameters is necessary not only to better
121 determine the final states, but also to evaluate time periods during which such final states are
122 reached. The analysis of time evolution is practically important because many DSDs measured
123 in-situ correspond to the transient state, but not to the final equilibrium state. Besides, it is
124 necessary to determine the evolution of initially polydisperse DSD, that may substantially differ
125 from the evolution of monodisperse DSD.

126 We analyze the time evolution of the DSD during homogeneous mixing in cases of
127 monodisperse and polydisperse initial DSDs. The analysis is based on new equations and
128 methodology developed by Pinsky et al. (2013, 2014).

129 First, we need to evaluate conditions at which mixing can be considered homogeneous. The
130 characteristic spatial scale of homogeneous mixing can be estimated by comparing the

characteristic times of two processes providing thermodynamic equilibrium inside a mixing volume. The first process is mechanical mixing (diffusion) governed by turbulence. Turbulent mixing leads to homogenization of temperature, humidity (and, thus, of supersaturation) as well as of droplet concentration within the volume $V = V_1 + V_2$. The second process is evaporation of a droplet ensemble, which leads to an increase in relative humidity and to the thermodynamical equilibrium in the mixing volume.

The process of mixing that is accompanied by droplet evaporation is characterized by two time scales. The first time scale is the characteristic mixing (homogenization) time τ_{mix} of an entrained volume with linear scale L_{mix} can be evaluated from the relationship (Monin and Yaglom, 1975)

$$\tau_{mix} = \varepsilon^{-1/3} L_{mix}^{2/3} \quad , \qquad (1)$$

where ε is the turbulent kinetic energy dissipation rate. The estimation (1) suggests that the size of the volume falls within the inertial interval of turbulence. Therefore, after the time τ_{mix}, volume with a linear scale of about L_{mix} will be mechanically homogenized and all the droplets in the volume will experience the same supersaturation.

The second time scale characterizes rate of droplet evaporation and corresponding changes of supersaturation. In this study, as well as later in Part.3, it will be shown that the characteristic evaporation time is the *phase relaxation time* τ_{pr}, that determines the rate of change of supersaturation during condensation or evaporation (Mazin, 1968; Korolev and Mazin, 2003)

$$\tau_{pr} = \left(4\pi \mathscr{D} \bar{r} N\right)^{-1}, \qquad (2)$$

where $N = N_{m0}$ is the concentration of droplets in the mixing volume, $\bar{r}$ is the mean radius of droplets and $\mathscr{D}$ is the diffusivity of water vapor. The spatial scale at which the mixing time is

153 equal to the phase relaxation time is called a phase relaxation scale L_{pr} (Mazin, 1968). This scale
154 can be calculated from Eqs. (1) and (2) as

155 $$L_{pr} = \varepsilon^{1/2}\tau_{pr}^{3/2} \approx \varepsilon^{1/2}\left(4\pi\mathscr{D}\bar{r}N\right)^{-3/2} \quad (3)$$

156 The type of mixing is often characterized by the value of the Damköhler number which in
157 regard to atmospheric mixing is defined as the ratio τ_{mix}/τ_{pr} (Baker et al., 1980; Jeffery, 2007;
158 Lehmann et al., 2009):
159

160 $$Da = \frac{\tau_{mix}}{\tau_{pr}} = \frac{4\pi\mathscr{D}\bar{r}NL_{mix}^{2/3}}{\varepsilon^{1/3}} \quad (4)$$

161 The case $Da << 1$ corresponds to homogeneous mixing, when mechanical homogenization
162 occurs much faster than does droplet evaporation. The case $Da >> 1$ corresponds to extremely
163 inhomogeneous mixing. It is reasonable to consider the value $Da = 1$ as a boundary separating
164 the two types of mixing. This condition is equivalent to the condition
165

166 $$L_{mix} = L_{pr} \approx \varepsilon^{1/2}\left(4\pi\mathscr{D}\bar{r}N\right)^{-3/2} \quad (5)$$

167

168 Expression (5) determines the maximum spatial scale at which mixing can be considered as
169 homogeneous. The evaluation of the spatial scales at conditions typical of different cloud types
170 is presented in **Table 1**. One can see that the characteristic volume size at which mixing can be
171 considered homogeneous ranges from 0.2 m to 0.6 m. At larger scales, supersaturation within the
172 mixing volume is non-uniform and droplets in the volume experience different values of relative
173 humidity. In this case, the mixing should be considered inhomogeneous.

174 The further paper structure is the following. In Section 2 we calculate the thermodynamic
175 characteristics of the resulting volume at the end of the first stage of mixing (see Fig. 1b).

176 Section 3 presents an analytic solution of homogeneous droplet evaporation in the monodisperse
177 DSD case. In Section 4 effects of polydispersivity on the DSD evolution are described. The
178 problem of turbulent mixing representation in numerical cloud models is discussed in Section 5.
179 The main results of the study are presented in Conclusion Section 6.
180

181 **2. Thermodynamic characteristics of the mixing volume at the end of the first stage**

182 At the first stage (see the scheme in Fig.1) homogeneous mixing is considered as an isobaric
183 process that is not accompanied by phase transitions (Korolev and Isaac, 2000). Let us consider
184 mixing between a cloud volume with mass m_1, supersaturation $S_1 = 0$ and temperature T_1 and a
185 droplet-free volume with mass m_2, supersaturation $S_2 < 0$ and temperature T_2. The cloud
186 volume also contains droplets with concentration N_1 and liquid water mixing ratio q_1 (Fig. 1).
187 For the sake of simplicity, we assume that the mass of both volumes is equal to one. Let us
188 further assume that μ is the mass fraction of the cloud air that mixes with the mass fraction
189 $(1-\mu)$ of the droplet-free air. In this case, the air mass in the mixing volume will be equal to
190 $m_1\mu + (1-\mu)m_2 = 1$. Isobaric mixing leads to an approximate linear dependence of droplet
191 concentration N_{m0} on μ.

192 After an instantaneous homogenization of the two volumes, the intermediate temperature
193 T_{m0}, droplet concentration N_{m0} and liquid mixing ratio q_{m0} are (see Pt.1):

194 $$N_{m0} = N_1\mu; \quad q_{m0} = q_1\mu; \quad T_0 = T_1\mu + T_2(1-\mu) \qquad (6a)$$

195 If the temperature difference $|T_1 - T_2|$ does not exceed a few degrees, the intermediate
196 supersaturation S_{m0} can be approximated by a linear dependence on μ

197 $$S_{m0} = S_2(1-\mu) \qquad (6b)$$

198 **Figure 2** shows, that in case $|T_1 - T_2| < 2^{o}C$, the deviations of supersaturation from the linear
199 dependence (6b) are small enough and can be neglected. In cases when the temperature of the
200 dry volume substantially differs from the temperature of the cloud volume, the dependence of the
201 resulting supersaturation on parameter μ becomes non-linear (Fig. 2). At temperature
202 differences of 5-10 ^{o}C, the deviation from the analytical solution (6) increases, which requires
203 using more precise formulas for supersaturation (see Pt. 1). Values of N_{m0}, q_{m0}, T_{m0} and S_{m0}
204 determine the initial conditions for the second stage of homogeneous mixing. This is actually
205 homogeneous evaporation of droplets, which leads to a thermodynamic equilibrium between
206 water vapor and liquid water.
207
208 **3. Analysis of homogeneous droplet evaporation in the monodisperse DSD case**
209
210 **3.1. Basic assumptions and equations**
211 The second stage of mixing consists in homogeneous evaporation of droplets. The evolution
212 of DSD during the second stage is considered here under the following assumptions: a) the
213 processes inside the mixing volume are adiabatic, b) the droplet size distribution is
214 monodisperse, c) the vertical velocity of the volume $u_z = 0$ and d) the sedimentation of droplets
215 is neglected and their concentration remains constant.
216 The liquid water mixing ratio can be expressed as
217 $$q(t) = \frac{4\pi\rho_w}{3\rho_a} N r^3(t) \qquad (7)$$
218
219 where $r(t)$ is the radius of droplets and N is the droplet number concentration. Closed
220 equations describing condensation/evaporation in a moving adiabatic air volume were obtained

by Pinsky et al. (2013). In an unmoving adiabatic volume, evaporation is described by the equation for supersaturation (e.g., Korolev and Mazin, 2003)

$$\frac{1}{S+1}\frac{dS}{dt} = -A_2\frac{dq}{dt} \tag{8}$$

and droplet evaporation is described by the simplified equation (Pruppacher and Klett, 2007)

$$r\frac{dr}{dt} = \frac{S}{F}, \tag{9}$$

where S is the supersaturation over a flat water surface. For cloud droplets Eq. (9) is valid with high accuracy. We do take into account formation of haze particles resulting from droplet evaporation. This allows us to neglect the curvature term and chemical term in the evaporation equation. Coefficients A_2 and F in Eqs. (8, 9) are slightly dependent on the temperature and the pressure

$$A_2 = \frac{1}{q_v} + \frac{L^2}{c_p R_v T^2} \tag{10}$$

$$F = \frac{\rho_w L^2}{k_a R_v T^2} + \frac{\rho_w R_v T}{e_S(T)\mathscr{D}} \tag{11}$$

We assume that coefficients A_2 and F do not change in the course of droplet evaporation.

The physical meaning and units of other variables are given in **Appendix A.**

3.2. Time evolution of supersaturation and of liquid water content

The closed differential equations for the liquid water mixing ratio q and supersaturation S to be used in the analysis are derived in **Appendix B.**

$$\frac{dq}{dt} = BN_{m0}^{2/3}\left[(S_{m0}+1)\exp\{-A_2(q-q_{m0})\}-1\right]q^{1/3} \tag{12}$$

$$\frac{1}{S+1}\frac{dS}{dt} = -A_2 BN_{m0}^{2/3} S\left(q_{m0} - \frac{1}{A_2}\ln\frac{S+1}{S_{m0}+1}\right)^{1/3} \tag{13}$$

where

$$B = \frac{3}{F}\left(\frac{4\pi\rho_w}{3\rho_a}\right)^{2/3} = const \qquad (14)$$

The solutions of these equations depend on the values of N_{m0}, q_{m0}, T_{m0}, and S_{m0}, obtained after the first stage of mixing. Eqs. (12) and (13) are rigidly connected by the following equation directly following from Eq. (8):

$$\ln[S(t)+1] = -A_2 q(t) + C \qquad (15)$$

where $C = \ln[S_{m0}+1] + A_2 q_{m0}$ is determined by the initial conditions at $t = 0$.

Since in this study we assume $S(t) \le 0$, it is convenient to use the relative humidity RH and the saturation deficit SD to characterize the thermodynamic state of the mixing volume. Both quantities are easily related to $S(t)$: $SD(t) = -S(t)$, $RH(t) = 1 + S(t)$. **Figure 3** demonstrates dependencies $S(t)$ and $q(t)$, calculated at an initial relative humidity RH_0 that varies from 72% to 91.6%, and an initial LWC of 0.6 gm^{-3}. RH_{m0} corresponds to the relative humidity in dry volume RH_2, that ranges from 43% to 83% at $\mu = 0.5$. The results of solving Eqs. (14-15) were compared with those obtained using a parcel model (Korolev, 1995) in which evaporation is described using equations with temperature-dependent parameters, and were found to be in excellent agreement. This agreement can be attributed to the fact that temperature changes that occurred in the course of the mixing are relatively small, validating the assumption about the constancy of A_2 and F.

As seen from Fig. 3, the final equilibrium state may be reached within several seconds. Fig. 3 shows the possibility of the two final states mentioned above: a) complete droplet evaporation

reached at different time instances depending on the initial value of S_{m0}, and b) partial droplet evaporation at $RH_{m0} > 82\%$. In the latter case, the final supersaturation is equal to zero.

3.3. Universal dependencies of supersaturation and of LWC on time

In order to simplify the further analysis we introduce the following non-dimensional parameters: normalized liquid water mixing ratio $\tilde{q} = \frac{q}{q_{m0}}$ which is equal to normalized liquid water content, normalized supersaturation $\tilde{S} = \frac{S}{A_2 q_{m0}}$, and non-dimensional time $t = t/\tau_{m0}$, where $\tau_{m0} = \left(BA_2 N_{m0}^{2/3} q_{m0}^{1/3}\right)^{-1}$ is the time scale. Then the set of non-dimensional equations describing changes of supersaturation and liquid mixing ratio can be written as (see Appendix B for detail)

$$\tilde{S}(\tilde{t}) = -\tilde{q}(\tilde{t}) + \gamma \tag{16}$$

$$\frac{d\tilde{q}}{d\tilde{t}} = \tilde{q}^{1/3}\left(\gamma - \tilde{q}\right) \tag{17}$$

$$\frac{d\tilde{S}}{d\tilde{t}} = -(\gamma - \tilde{S})^{1/3}\tilde{S}, \tag{18}$$

where

$$\gamma = 1 + \frac{S_{m0}}{A_2 q_{m0}} = 1 + \frac{1-\mu}{\mu}\frac{S_2}{A_2 q_1} \tag{19}$$

is dimensionless parameter which depends on the initial supersaturation S_{m0} and the initial liquid water mixing ratio q_{m0}. The value of this parameter can be either positive or negative. Eqs. (16-18) are strictly valid if $|S_{m0}| << 1$, i.e. when the value of supersaturation S is negligible in comparison with unity in the factor $(S+1)^{-1}$ on the left-hand side of Eq. (8). However, a detailed comparison of solutions of Eqs. (16-18) with those obtained using a numerical model showed

that Eqs. (16-18) provide accurate solution at RH_{m0} as low as 30-40%. Eq. (17) should be solved with the initial condition $\tilde{q}(0)=1$, and Eq. (18) should be solved with the initial condition $\tilde{S}(0)=\dfrac{S_{m0}}{A_2 q_{m0}}<0$. Therefore, solutions of both equations depend on the sole parameter γ. Eqs. (17) and (18) are rigidly connected by balance equation Eq. (16).

Defining $x(\tilde{t})=\left(\tilde{q}(\tilde{t})\right)^{1/3}$ and $\chi=|\gamma|^{1/3}\mathrm{sgn}(\gamma)$, the solution of Eq. (17) with the initial condition $x(0)=1$ is

$$2\chi\tilde{t}=\ln\left[\frac{(1-\chi)^2}{(x-\chi)^2}\frac{x^2+\chi x+\chi^2}{1+\chi+\chi^2}\right]+2\sqrt{3}\left[\operatorname{atan}\frac{2\sqrt{3}\chi(1-x)}{3\chi^2+(2+\chi)(2x+\chi)}\right] \qquad (20)$$

The solution for the normalized supersaturation can be obtained from Eq. (20) and the balance equation (16)

$$\tilde{S}(\tilde{t})=-\tilde{q}(\tilde{t})+\gamma=-x^3(\tilde{t})+\chi^3 \qquad (21)$$

Figure 4 demonstrates time dependencies $\tilde{S}(\tilde{t})$ and $\tilde{q}(\tilde{t})$ calculated at different γ at $S_{m0}>-10\%$ (i.e. $RH_{m0}>90\%$). As seen from Fig. 4. the analytical solution is quite close to the numerical one. The deviation increases with a decrease in parameter γ. At $\gamma=-0.5$, the error in the final *RH* is about 15%. The initial RH_{m0} in this case is about 90 %. RH_{m0} is the relative humidity in the mixing volume V after the first stage of mixing. As mentioned above, RH_{m0} may be substantially higher than RH_2 in the initially droplet-free volume. *In-situ* measurements (Gerber et al., 2008) and remote measurements of aerosol humidification (Knight and Miller, 1998; Bar-Or et al., 2012) indicate the existence of zones of high *RH* along cloud edges. These observations and results of numerical simulations indicate that the analytical solution (20-21) is a universal one and applicable at any RH values in cloud surrounding.

303 The amplitude of the deviation of the analytical solution for supersaturation from the
304 modeled result decreases with the decrease of γ. The cause of the deviation is neglecting term
305 $(S+1)$ on the left-hand side of Eq. (8).

306 There are two types of solutions determined by parameter χ (or parameter γ), separated by
307 value $\chi = 0$ (Figs. 3 and 4). Condition $\chi = 0$ corresponds to $\mu = \mu_{cr}$ (see Pt 1) and indicates
308 complete evaporation of all the droplets and the relative humidity increasing up to 100 %.
309 Condition $\chi > 0$ corresponds to solutions $\tilde{q}(\tilde{t})$ with asymptotic behavior at $\tilde{t} \to \infty$: $\tilde{q} \to \gamma$ and
310 $\tilde{S} \to 0$, which means that droplets do not completely evaporate. Condition $\chi < 0$ means that all
311 the droplets completely evaporate.

312 At $\chi = 0$, the analytical solution is:

313 $$x = \frac{3}{\tilde{t}+3}; \quad \tilde{q}(\tilde{t}) = \left(\frac{3}{\tilde{t}+3}\right)^3; \quad \tilde{S}(\tilde{t}) = -\left(\frac{3}{\tilde{t}+3}\right)^3 \qquad (22)$$

314 Both LWC and supersaturation tend to zero at $\tilde{t} \to \infty$.

315 At $\chi < 0$, the duration of the evaporation is limited in time (Figs. 3, 4). Normalized
316 evaporation time t_e depends on parameter χ only. This dependence can be obtained from Eq.
317 (20) at $x = 0$:

318 $$t_e = \frac{1}{2\chi} \ln \frac{(1-\chi)^2}{1+\chi+\chi^2} + \frac{\sqrt{3}}{\chi} \operatorname{atan} \frac{\sqrt{3}}{2\chi+1} \qquad (23)$$

319 Here the time is counted in the relaxation time scales. This fact indicates that the phase
320 relaxation time is the time scale that should be used in the analysis of mixing. The choice of a
321 time scale will be discussed elaborated in greater detail below.

322 At $\chi > -1/2$, one have to use the values $\operatorname{atan}\left(\frac{\sqrt{3}}{2\chi+1}\right)-\pi$ in Eq. (23) instead of $\operatorname{atan}\frac{\sqrt{3}}{2\chi+1}$.

323 t_e is the time needed for supersaturation to reach its maximal value (Figs. 3a, 4a). This value is

324 calculated from Eqs. (16) and (6)

325 $$\tilde{S}_{\max} = \gamma = \chi^3 = 1 + \frac{S_{m0}}{A_2 q_{m0}} \approx 1 + \frac{S_2}{A_2 q_1}\frac{1-\mu}{\mu} = 1 + R\frac{1-\mu}{\mu} \qquad (24)$$

326 where $R = \frac{S_2}{A_2 q_1}$ is a dimensionless parameter describing the ratio of S_2 in the initially dry air

327 and the reserve of liquid water available for evaporation. (This parameter can be determined

328 more precisely using Eq. (2) or Eq. (4) given in Pt. 1). This parameter can be referred to as a

329 potential evaporation parameter (PEP). The PEP is proportional to the ratio of the amount of

330 water vapour that should evaporate in order to saturate the initially droplet-free volume (that is

331 determined by S_2) to the initial available liquid water q_1 in the cloud volume in case of equal

332 initial volumes $V_1 = V_2$.

333 The dependence $t_e(\chi)$ is shown in **Figure 5. O**ne can see that at large sub-saturation values

334 ($\chi < -0.4$) all the droplets evaporate within the span of a few relaxation times, and the analytical

335 results agree well with the model (benchmark) results. At a high initial *RH*, droplet evaporation

336 increases the humidity to nearly the saturation value, at which evaporation becomes extremely

337 slow. In this case, simplified analytical formulas overestimate the evaporation time.

338 At $\chi > 0$, droplets partially evaporate, q reaches the minimal value and the thermodynamic

339 equilibrium is reached when $S \to 0$. Minimal normalized equilibrium LWC can be found from

340 Eqs. (21) and (6)

341 $$\tilde{q}_{\min} = \gamma = \chi^3 = 1 + R\frac{1-\mu}{\mu} \qquad (25)$$

342 Eq. (25) is similar to Eqs. (4-5) (see Pt.1.).

Dependences of $\tilde{S}_{\max}$ and $\tilde{q}_{\min}$ on cloud air fraction, calculated at different initial conditions using Eqs. (24) and (25) are shown in **Figure 6**. The diagram in Fig. 6b is actually a kind of widely used mixing diagram for homogeneous mixing, and Eq. (25) is an universal analytic equation for calculation of this diagram depending on the non-dimensional parameter R. Panel (a) shows that the higher the cloud fraction of air parcels involved in mixing, the lower the saturation deficit, i.e. the higher the final *RH* is. At small R, saturation is reached at a low μ. Similar diagrams in physical units are shown in Pt.1 in Figs. 4a,g.

The equations presented above allow to predict the results of homogeneous mixing both for partial and complete evaporation of droplets (**Table 2)**. One can see that at low temperatures, the environment air volume becomes cloudy at relatively low values of liquid water content in the cloud volume even if *RH* of the environment volume is as low as 50%. The reason is that the saturation ratio at low temperatures is low and only a small amount of liquid should be evaporated to make the initially dry volume saturated.

The diagram in Fig.6b allows to calculate the final liquid water content remaining in the entire volume after saturation reaches 100%. This diagram also shows that for each value of μ there is a certain value of R at which full evaporation takes place. The remaining $\tilde{q}_{\min}$ increases with decreasing q_1 and increasing RH_2, as shown by the arrow.

The natural time scale of the evaporation and, therefore, homogeneous mixing was determined as $\tau_{m0} = \left(BA_2 N_{m0}{}^{2/3} q_{m0}^{1/3}\right)^{-1}$. This value is inversely proportional to $N_{m0} r_{m0}$ and actually coincides with the initial phase relaxation time τ_{pr}. The equality of the characteristic time scales of variations in supersaturation and in liquid water content directly follows from the equation (15). Indeed, in case of $|S| << 1$ the equation can be rewritten as $S(t) = -A_2 q(t) + C$ thus establishing a linear relationship between the supersaturation and the liquid water mixing ratio.

366 It should be emphasized that τ_{m0} is not the time of total droplet evaporation or the time of
367 reaching saturation (when evaporation is over). The time of complete evaporation of all droplets
368 can be substantially longer than phase relaxation time τ_{m0}.

369

370 **4. Analysis of homogeneous droplet evaporation in case of a polydisperse DSD**

371 **4.1. DSD evolution in the course of droplet evaporation**

372 To analyse polydisperse DSD evolution during droplet evaporation at the second stage of
373 homogeneous mixing, we use the same equations for diffusional growth (9) and supersaturation
374 (8) as those used in case of a monodisperse DSD. The solution of Eq. (9) can be written in the
375 form

376 $$r^2(t) = r_0^2 - Q(t) \qquad (26)$$

377 where the non-negative function $Q(t) \geq 0$ is proportional to the supersaturation integral

378 $$Q(t) = -\frac{2}{F}\int_0^t S(t')dt' \geq 0 \qquad (27)$$

379 This function characterizes a decrease in the square of droplet radii. At $t = 0$, $Q(0) = 0$. Let
380 $f_0(r_0)$ be an initial DSD immediately following the first stage of homogeneous mixing. This
381 distribution obeys the normalization condition

382 $$N_{m0} = \int_0^\infty f_0(r_0)dr_0 \qquad (28)$$

383 where N_{m0} is the initial droplet number concentration after the first stage of mixing. Using the
384 inverse transformation $r_0 = \sqrt{r^2 + Q(t)}$ alongside with condition $r \geq 0$ and the relation between
385 the distribution functions $f(r,t) = f_0(r_0)\frac{dr_0}{dr}$ we get

$$f(r,t)=\begin{cases}\dfrac{r}{\sqrt{r^2+Q(t)}}\,f_0\left(\sqrt{r^2+Q(t)}\right), & r\ge 0\\ 0, & r<0\end{cases} \tag{29}$$

Eq. (29) shows that the time changes in DSD and in its moments depend both on the initial DSD at $t=0$, $f_0(r_0)$ and on the time-dependent function $Q(t)\ge 0$.

To illustrate the DSD evolution using Eq. (29), we assume that the initial distribution immediately following the first stage of mixing can be represented by a Gamma distribution:

$$f_0(r_0)=\frac{N_{m0}}{\Gamma(\alpha)\beta}\left(\frac{r_0}{\beta}\right)^{\alpha-1}\exp\left(-\frac{r_0}{\beta}\right) \tag{30}$$

where N_{m0} is an intercept parameter, α is a shape parameter and β is a slope parameter of distribution. Different sets of parameters allow approximations of both narrow and wide DSD. The parameters of the initial Gamma distribution used in this study are presented in **Table 3** and are chosen so that the modal radii of DSD and the LWC would be the same for both distributions.

Combining Eqs. (29) and (30) yields an equation for DSD evolution as a function of $Q(t)$

$$f(r,t)=\begin{cases}\dfrac{N_{m0}}{\Gamma(\alpha)\beta^{\alpha}}(r^2+Q)^{\frac{\alpha}{2}-1}\,r\exp\left(-\dfrac{\sqrt{r^2+Q}}{\beta}\right), & r\ge 0\\ 0, & r<0\end{cases} \tag{31}$$

This DSD (31) depends on four parameters, wherein parameter $Q(t)$ increases with time according to Eq. (27). Examples of evolutions of an initially narrow DSD and an initially wide DSD are shown in **Figure 7**. All the calculations were performed using a parcel model (Korolev, 1995).

There is a significant difference between evolution of DSDs in cases of monodisperse and polydisperse DSDs. At a monodisperse DSD, droplet concentration remains unchanged until the final stage of evaporation when droplets become small and then all evaporate rapidly. At a

406 polydisperse DSD the droplet concentration decreases simultaneously with the decrease in
407 LWC. Evaporation of a the narrow size distribution is consistent with the concept of
408 homogeneous mixing (Fig. 7a). However homogeneous evaporation of droplets with a wide
409 DSD may be mistakenly taken for inhomogeneous mixing.
410

411 **4.2. Evolution of DSD moments and related functions**

412 Eq. (29) also allows evaluation of droplet concentration, DSD moments and related
413 functions. Droplet concentration corresponds to the zero moment of DSD and can be expressed
414 as

415 $$N(t)=\int_0^\infty f(r,t)dr=\int_0^\infty \frac{r}{\sqrt{r^2+Q(t)}}\, f_0\left(\sqrt{r^2+Q(t)}\right)dr=\int_{\sqrt{Q(t)}}^\infty f_0(r_0)dr_0 \qquad (32)$$

416 Since function $Q(t)$ monotonically increases with the time, the right-hand integral in Eq. (32)
417 decreases, indicating a decrease in droplet concentration with time. If the initial distribution of
418 droplets is described by a Gamma distribution, the decrease of droplet concentration with the
419 time is evaluated using Eqs. (30) and (32) as

420 $$N(t)=\int_{\sqrt{Q(t)}}^\infty f_0(r_0,t)dr_0=\int_{\sqrt{Q(t)}}^\infty \frac{N_{m0}}{\Gamma(\alpha)\beta}\left(\frac{r_0}{\beta}\right)^{\alpha-1}\exp\left(-\frac{r_0}{\beta}\right)dr_0=$$

421 $$\frac{N_{m0}}{\Gamma(\alpha)}\int_{\frac{\sqrt{Q(t)}}{\beta}}^\infty x^{\alpha-1}\exp(-x)dx=N_{m0}\frac{\Gamma(\alpha,\eta)}{\Gamma(\alpha)}. \qquad (33)$$

422

423 where

424 $$\eta(t)=\frac{\sqrt{Q(t)}}{\beta} \qquad (34)$$

425 is a non-dimensional function of time and $\Gamma(\alpha,\eta(t))$ is an upper incomplete Gamma function
426 (Korn and Korn, 2000). It follows from Eqs. (32) and (33) that $N(t)\le N_0$. The dependencies of

427 the normalized droplet concentration $\frac{N(t)}{N_{m0}}$ on time for an initially narrow DSD and an initially

428 wide DSD are shown in **Figure 8**.

429 Fig. 8 shows that in case of an initially narrow DSD, droplet concentration does not change

430 during the first 20 s when $RH_0 = 91.6\ \%$ because the DSD does not shift strongly enough

431 toward smaller droplet radii. At lower initial supersaturations, droplet concentration decreases

432 with time. This decrease may take place rapidly and may last several seconds only. The red line

433 separates two different evaporation scenarios. The curves above the red line correspond to partial

434 evaporation and reaching the saturation state, whereas the curves below the red line correspond

435 to complete evaporation of droplets and the environment remains subsaturated.

436 At an initially wide DSD, droplet concentration decreases at any initial subsaturation value

437 because the DSD contains small droplets that start evaporating regardless the subsaturation

438 value. In the particular example shown in Fig. 8, the droplet relaxation time is shorter in case of a

439 wide DSD, so droplet concentration decreases slower than at a narrow DSD. Droplet

440 concentration decreases substantially during a few tens of seconds, but does not reach zero due

441 to a significant concentration of large droplets in the wide DSD. The equilibrium state is not

442 reached within 20 s.

443 Fig. 8 also demonstrates an excellent agreement between the results of analytical calculations

444 performed using Eq. (33) and results obtained using the parcel model.

445 A normalized moment of the *k-th* order is evaluated as

446
$$\overline{r^k(t)} = \frac{1}{N(t)}\int_0^\infty r^k f(r,t)dr = \frac{1}{N(t)}\int_0^\infty \frac{r^{k+1}}{\sqrt{r^2+Q(t)}} f_0\left(\sqrt{r^2+Q(t)}\right)dr = \frac{1}{N(t)}\int_{\sqrt{Q(t)}}^\infty \left(r_0^2 - Q(t)\right)^{k/2} f_0(r_0)dr_0$$

447

448 $$\overline{r^k}(t) = \frac{\int_{\sqrt{Q(t)}}^{\infty} \left(r_0^2 - Q(t)\right)^{k/2} f_0(r_0) dr_0}{\int_{\sqrt{Q(t)}}^{\infty} f_0(r_0) dr_0} \qquad (35)$$

449 In case when the initial distribution is given by the Gamma distribution (30), Eq. (35) leads to
450 the following equation

451 $$\overline{r^k}(t) = \frac{\beta^k}{\Gamma\left(\alpha, \eta(t)\right)} \int_{\eta(t)}^{\infty} \left(x^2 - \eta^2(t)\right)^{k/2} \left(x\right)^{\alpha-1} \exp\left(-x\right) dx \qquad (36)$$

452 The even moments can be represented using incomplete the Gamma functions.

453 **Figures 9 and 10** show the time dependencies of quantities typically used for characterizing
454 the DSD shape, namely the mean radius $\overline{r}(t)$ (panel (a)), the effective radius $r_{eff}(t) = \frac{\overline{r^3}(t)}{\overline{r^2}(t)}$
455 (panel (b)), the RMS width of DSD $\sigma(t) = \sqrt{\overline{r^2}(t) - \overline{r}^2(t)}$ (panel (c)) and the dispersion
456 coefficient $\delta(t) = \frac{\sigma(t)}{\overline{r}(t)}$ (panel (d)). The dependencies corresponding to an initially narrow DSD
457 are shown in Fig. 9 and those corresponding to an initially wide DSD are shown in Fig. 10.

458 At an initially narrow DSD, the mean radius and the effective radius decrease with time in
459 agreement with the concept of homogeneous mixing. Formation of plateaus in the mean radii, in
460 the effective radii and in droplet dispersion over long time periods is caused by the existence of
461 droplets in the tail of DSD distributions. While the concentration of such droplets is negligibly
462 small, their evaporation takes a significant amount of time.

463 At an initially wide DSD (Fig.7b), complete evaporation of the smallest droplets starts at the
464 very beginning of the second stage of mixing. This evaporation leads to an increase in the
465 effective radius and in the mean radius that changes non-monotonically. An increase in the
466 value of the effective radius contradicts the concept of homogeneous mixing, according to which
467 both the mean radii and the effective radii decrease in the course of mixing. This increase is

468 explained by the fact that subsaturation at an initially wide DSD leads to a significant rapid
469 decrease in the concentration of small droplets, while the changes in LWC whose value is
470 determined by larger droplets, do not occur that quickly.

471 The opposite behaviors of the effective radii (as well as of the other characteristic droplet
472 sizes) at a narrow DSD vs. a wide DSD, illustrated in Figs. 9 and 10, suggest the existence of a
473 large number of DSDs with initial shapes at which the evaporation of droplets leads to a decrease
474 in droplet concentration, but does not change significantly the effective radius. So the constancy
475 of the effective radius at varying droplet concentrations does not allow to distinguish the mixing
476 type with full confidence. Even at a narrow DSD, the decrease in the value of the effective radius
477 does not exceed 20% at the an initial saturation deficit of 8.4 %.

478 In any case the evolution of DSD and of their parameters is determined by the competition
479 between two effects. First, this is the effect of partial droplet evaporation which shifts the DSD
480 toward smaller sizes and leads to a decrease in the mean radii and in the effective radii, as well
481 as widens the DSD. Second, this is the effect of complete evaporation of the smallest droplets,
482 which increases both the mean radii and the effective radii. The relative contribution of these two
483 effects depends on the initial DSD width and the value of the mean radius. The best indicators of
484 these two effects are the DSD width, σ and the DSD dispersion $\frac{\sigma}{\overline{r}}$.

485 At an initially narrow DSD and an initially low *RH*, partial evaporation initially dominates
486 and the DSD width increases due to the appearance of smaller droplets (Fig. 9c). Afterwards,
487 when complete droplet evaporation becomes the dominant factor, the DSD shifts significantly to
488 small sizes and the DSD width decreases. At an initially large *RH*, complete droplet evaporation
489 is not efficient, and the DSD gets continuously wider. Since the mean radius decreases, the DSD
490 dispersion tends to constant values at any initial *RH*. However, the largest DSD dispersion takes
491 place at an initially low *RH*, when evaporation substantially decreases the mean droplet radius.

As seen in Figs. 9d and 10d, the initial DSD dispersion at a narrow DSD is 0.1, while the initial dispersion at a wide DSD is 0.5.

Figs. 10c and 10d show that at an initially wide DSD, homogeneous evaporation leads to an increase in both DSD width and DSD dispersion. The increase in the DSD width indicates that formation of the smallest droplets by partial evaporation is the main mechanism of the DSD shape evolution. The DSD dispersion increases with time and rapidly reaches quasi-stationary values of about 0.56 that are typical of real clouds.

4.3. Evolution of LWC and of supersaturation

Using Eq. (35), the time dependence of the liquid water mixing ratio is represented as

$$q(t) = \frac{4\pi\rho_w}{3\rho_a} N(t)\overline{r^3(t)} = \frac{4\pi\rho_w}{3\rho_a} \int\limits_{\sqrt{Q(t)}}^{\infty} \left(r_0^2 - Q(t)\right)^{3/2} f_0(r_0) dr_0 \qquad (37)$$

If the initial DSD is approximated by a Gamma distribution, $q(t)$ can be written as

$$q(t) = \frac{4\pi\rho_w}{3\rho_a} \int\limits_{\sqrt{Q(t)}}^{\infty} \left(r_0^2 - Q(t)\right)^{3/2} \frac{N_{m0}}{\Gamma(\alpha)\beta} \left(\frac{r_0}{\beta}\right)^{\alpha-1} \exp\left(-\frac{r_0}{\beta}\right) dr_0 =$$
$$\frac{4\pi\rho_w}{3\rho_a} \frac{N_{m0}\beta^3}{\Gamma(\alpha)} \int\limits_{\eta(t)}^{\infty} \left(x^2 - \eta^2(t)\right)^{3/2} (x)^{\alpha-1} \exp(-x) dx \qquad (38)$$

Since at $t = 0$, $\eta = 0$ and the initial liquid water mixing ratio is equal to $q_{m0} = \frac{4\pi\rho_w}{3\rho_a} N_{m0}\beta^3 \frac{\Gamma(\alpha+3)}{\Gamma(\alpha)}$, hence the normalized liquid water mixing ratio is calculated as

$$\frac{q(t)}{q_{m0}} = \frac{1}{\Gamma(\alpha+3)} \int\limits_{\eta(t)}^{\infty} \left(x^2 - \eta^2(t)\right)^{3/2} (x)^{\alpha-1} \exp(-x) dx \qquad (39)$$

Figure 11 shows the time dependencies of LWC for different initial RH_0 in the resulting volume (Fig.11a: an initially narrow DSD; Fig.11b: an initially wide DSD). One can see that at an initially narrow DSD the LWC rapidly decreases, either to zero (full evaporation) or, as in the

monodisperse case, to an equilibrium value during a time period of the phase relaxation time (see Section 3 for comparison). At an initially wide DSD, the LWC decreases slowly and monotonically. In general, at an initially narrow DSDs the time dependencies, $q_w(t)$ are quite close to those for monodisperse DSD (Fig. 3b). The higher the initial *RH*, the smaller the change in the LWC is.

To calculate the time dependencies of supersaturation, one can use the full equation (8) or Eq. (15) written in the form:

$$S(t) = (S_{m0} + 1)\exp\left\{-A_2\left[q(t) - q_{m0}\right]\right\} - 1 \qquad (40)$$

In Eq. (40), S_{m0} and q_{m0} are the initial supersaturation and the liquid water mixing ratio, respectively, at $t = 0$. The corresponding time dependencies are shown in **Figure 12.** The analytical results of Eq. (40) are compared with the exact numerical solution obtained by a parcel model, showing a good agreement. The behavior of supersaturation at a initially narrow DSD is similar to that of a monodisperse DSD (Fig. 3a). As in Fig. 3a, the equilibrium non-zero values of subsaturation correspond to complete droplet evaporation. At initially wide DSD, the saturation deficit monotonically decreases as a consequence of the monotonic decrease in the LWC.

Figure 13 shows the dependencies of normalized LWC on normalized droplets concentrations calculated at different values of the initial relative humidity RH_{m0} in the mixing volume ((a): the initially narrow DSD and (b) the initially wide DSD). Each point on the curves corresponds to a certain time. Since the dependencies are plotted in non-dimensional coordinates, the time instance $t = 0$ corresponds to coordinates (1, 1). The numbers along the curves denote the points corresponding to time instance $t = 20\,\text{s}$. At lower RH_0, the curves reach lower values of LWC and of droplet concentration. In case of an initially narrow DSD the curve can be divided into three sections. The first section corresponds to high RH_0 ($RH_0 > 90\%$).

Within this section, the droplet concentration does not decrease with decreasing LWC, which is in line with the conceptual scheme of homogeneous mixing (Fig. 1). This section corresponds to the straight horizontal line in Fig. 8a. At lower relative humidity, the droplet concentration begins to decrease with a decreasing LWC, in line with Fig. 8a. When the LWC reaches small values, the dependence of the normalized LWC on the normalized droplet concentration becomes close to linear. At an initially wide DSD (Fig. 13b), the dependence of the LWC on droplet concentration is close to linear at all the values of RH_0. This linear dependence means that the mean volume radius varies only slightly during droplet evaporation.

It is noteworthy that all the curves plotted for different initial values of RH_0 coincide. This coincidence can be explained by the fact that all the DSDs used depend on four parameters, namely, the three parameters of the initial Gamma distribution and on $Q(t)$ (Eq. 31). The parameters of Gamma distributions are identical for each panel in Fig. 13. Parameter $Q(t)$ monotonically increases with time. At different RH_0, the values of $Q(t)$ reach the same values at different times. When the values of $Q(t)$ are the same, the DSDs and all the DSD moments are equal.

To sum up, at an initially narrow DSD and a comparatively large initial relative humidity $RH_0 > 87\%$ phenomenon demonstrates properties typically attributed to homogeneous mixing, when a decrease in both the LWC and the effective radius takes place at unchanged droplet concentration (Figs. 8a, 9b, 11a, 13a). In contrast, in the case of an initially wide DSD, the evolution of the DSD and its moments is close to that typically attributed to inhomogeneous mixing, when droplet evaporation leads to a decrease in LWC and in droplet concentration, while the effective radius remains unchanged. During the changes of a wide DSD, its shape remains similar to itself (Fig. 7b), which is also considered typical of inhomogeneous mixing.

5. Discussion: Application of the concept of homogeneous mixing in numerical modeling

The procedure of mixing in any cloud model involves two steps. At the first step, the changes in microphysical values in each grid point are calculated using the turbulent flux divergences. In case mixing takes place between any two volumes represented by neighbouring grid points, the mixing volume containing both grid points never becomes homogeneous (*a fortiori*, the microphysical values in these grid points do not become identical during one time step), so the spatial gradients of the microphysical variables remain between neighbouring grid points. This step represents inhomogeneous mixing at resolving scales. Mixing algorithm in models does not operate with "final" equilibrium values, as assumed in the classical mixing concepts, but rather with current time-dependent values. In contrast, the changes in the microphysical and thermodynamical variables in the volumes represented by one grid points are often considered uniform at each time step, and therefore, the modelled subgrid mixing is treated as homogeneous. Therefore, in most numerical models mixing is inhomogeneous at resolved scales, but homogeneous at subgrid scales.

The estimations in Tab. 1 indicate that mixing is homogeneous at scales lower than ~0.5 m. This means that to simulate homogeneous mixing explicitly, the grid spacing should be less than 0.5 m. If such grid spacing is used, the separation between mixing types could be described explicitly. However, grid spacing in most models significantly exceeds this value. This fact brings up two questions: "What error is introduced when the spatial scale separating mixing types in models is much larger than 0.5 m?" and "Why are spectral microphysics models with a resolution of 40-50 m able to reproduce observed DSD and their moments with high accuracy (Benmoshe et al., 2012; Khain et al., 2013, 2015; Magaritz-Ronen et al., 2014)?"

There are several factors that compensate errors in segregating mixing types in cloud models and allow using grid scale $L > L_{pr}$ with little effect on DSD. The first factor is that mixing leads

585 to formation of cloud zones characterized by a spatial correlation scale (radius of correlation) of
586 temperature, humidity and droplet concentration of about 150-250 m (Magaritz-Ronen et al.,
587 2014). Numerical experiments with Lagrangian-Eulerian model of Sc (Magaritz-Ronen et al.,
588 2014) have shown that the results are not sensitive to the choice of parcel size, if this size is
589 substantially smaller than the spatial radius of correlation. Therefore, the mixing type has a
590 minor effect on the results of mixing at scales lower than the radius of correlation.

591 The second factor is that in-cloud mixing often takes place at conditions close to saturation.
592 At such high humidity, homogeneous and inhomogeneous mixing yield practically the same
593 results. The similarity of results for the two mixing types is due to the fact that mixing in clouds
594 is not accompanied by an appreciable phase transition.

595 The third factor was pointed out by Hill et al. (2009), who explained that stratocumulus cloud
596 evolution is insensitive to the type of sub-grid mixing since the rates of condensation/evaporation
597 caused by the resolved dynamics are by two orders of magnitude greater than the
598 condensation/evaporation rate caused by the sub-grid processes.

599 The fourth factor that permits us to treat sub-grid mixing as homogeneous near cloud
600 interfaces is that DSDs are polydisperse, which is opposite what is assumed in the conventional
601 mixing considerations. In the present study it was shown that for a broad DSD, the changes of
602 r_{eff} remain small during mixing. So, a relatively small partial evaporation of droplets provide
603 sufficient amount of water vapor for saturation of the volume. In this case homogeneous mixing
604 becomes indistinguishable from inhomogeneous. The saturation of the volume may be facilitated
605 by entrainment of water vapor from neighboring cloud volumes.
606

607 **6. Conclusions**
608

609 The present study is focused on the dynamics of DSD transformation during the evaporation
610 stage of homogeneous mixing. The results can be summarized as follows.

611 1. Analytical equations describing time evolution of normalized supersaturation and
612 normalized LWC are obtained. It is found that these time dependences are universal functions
613 of a sole non-dimensional parameter $\gamma = 1 + \frac{S_{m0}}{A_2 q_{m0}}$. In particular, the dependences of normalized
614 LWC at the final stage on the cloud air fraction, used for plotting the universal mixing diagrams,
615 are obtained analytically. These diagrams also depend on a sole non-dimensional parameter
616 $R = \frac{S_2}{A_2 q_1} < 0$, which is proportional to supersaturation in dry volume and inversely proportional
617 to liquid water mixing ratio in a cloud volume. This parameter is uniquely related with parameter
618 γ by Eq. (24). It is shown that in many cases the major changes in the LWC take place during
619 the time period of the order of the phase relaxation time τ_{pr}. The equilibrium state can be
620 reached after several τ_{pr} periods.

621 2. It is shown that the phase relaxation time is a natural time scale of mixing process. This is
622 clearly seen from the universal renormalized evaporation equations, in which the phase
623 relaxation time plays the role of a time unit. In some studies (e.g. Baker and Latham, 1979;
624 Burnet and Brenguier, 2007; Andejchuk et al., 2009) evaporation time for an individual droplet
625 under given sub-saturation is considered as a characteristic time of mixing. The present study
626 shows that only the phase relaxation time should be used as the characteristic time scale of
627 mixing since we have to consider the behavior of a large amount of droplets. Supersaturation (or
628 sub-saturation) is not a parameter that determines the phase relaxation time. Thus, the utilization
629 of the evaporation time of individual droplet (at unchanged supersaturation) as the characteristic
630 time scale of mixing is physically ungrounded. A strict relationship between the changes in

631 supersaturation and in the liquid water mixing ratio makes it impossible to consider the changes
632 in an individual droplet size and in supersaturation independently.

633 3. An important outcome of this study is demonstration of a significant difference in the
634 evaporative behavior between narrow DSD and wide DSD. It is shown that homogeneous
635 evaporation of a wide DSD is accompanied by reduction in LWC and in droplet concentration
636 due to total evaporation of small droplets. Such changes of LWC and droplet concentration are
637 qualitatively different from those in the classic concept of homogeneous mixing. As a result,
638 homogeneous mixing may be erroneously interpreted as inhomogeneous one.

639 4. It is shown that the evolution of DSDs and their moments in case of polydisperse DSDs,
640 can qualitatively differ from that predicted by homogeneous mixing concept. Evaporation of a
641 comparatively wide DSD may even lead to an increase in the effective radii and DSD high
642 moments. This feature is typically attributed to inhomogeneous mixing.

643 Note that the role of DSD polydispersity in the mixing process is different from that in
644 diffusion droplet growth in ascending parcels. In an ascending adiabatic parcel the
645 supersaturation tends to zero with height, and the DSD width decreases with height as well. In
646 this case, it is possible to reproduce the height dependencies and the time dependencies of
647 supersaturation and of LWC using an "equivalent" monodisperse DSD with the same droplet
648 concentration as a polydisperse DSDs (Pinsky et al., 2014). As regards to mixing with a
649 polydisperse DSD, it cannot be reproduced using a monodisperse DSD, with a possible
650 exception in case of an initially extremely narrow DSD.

651

652 ***Acknowledgements.*** This research was supported by the Israel Science Foundation (grant
653 1393/14), the Office of Science (BER), the US Department of Energy Award DE-SC0006788
654 and the Binational US-Israel Science foundation (grant 2010446). Dr. Korolev's participation
655 was supported by Environment Canada.

656

657

658 **Appendix A: List of Symbols**

659

660 **Table A1 here**

661

662

663 **Appendix B. Derivation of closed equations for supersaturation and for liquid water**
664 **mixing ratio in the monodisperse DSD case.**

665

666 Let us consider motionless well-mixed adiabatic air volume having an initial supersaturation
667 $S_{m0} < 0$ and an initial liquid water mixing ratio q_{m0}.

668 1. Substitution of the formula of the liquid water mixing ratio $q = \frac{4\pi\rho_w}{3\rho_a} N r^3$ into the
669 equation for droplet radius evolution

670 $$r\frac{dr}{dt} = \frac{S}{F} \qquad \text{(B1)}$$

671 leads to the equation for the decrease of q with the time

672 $$\frac{dq}{dt} = \frac{3}{F}\left(\frac{4\pi\rho_w}{3\rho_a}\right)^{2/3} N^{2/3} S q^{1/3} = B N^{2/3} S q^{1/3} \qquad \text{(B2)}$$

673 where

674 $$B = \frac{3}{F}\left(\frac{4\pi\rho_w}{3\rho_a}\right)^{2/3} = const \qquad \text{(B3)}$$

675 2. Equation for supersaturation is written as (Korolev and Mazin, 2003)

676 $$\frac{1}{S+1}\frac{dS}{dt} = -A_2\frac{dq}{dt} \qquad \text{(B4)}$$

677 Integration of this equation under the assumption that $A_2 = const$ leads to the equation

678 $$\ln\left[S(t)+1\right] = -A_2 q(t) + C \qquad \text{(B5)}$$

679 where C is determined by initial conditions at $t = 0$

680 $$C = \ln(S_{m0}+1) + A_2 q_{m0} \qquad \text{(B6)}$$

681 Using Eqs. (B5) and (B6) one obtains the equation with respect to $S(t)$

682 $$S(t) = (S_{m0}+1)\exp\left\{-A_2\left[q(t)-q_{m0}\right]\right\} - 1 \qquad \text{(B7)}$$

683 3. Mutual substitution of Eqs. (B2) and (B7) leads to the closed differential equations for
684 $q(t)$ and $S(t)$

685 $$\frac{dq}{dt} = BN^{2/3}\left[(S_{m0}+1)\exp\left\{-A_2(q-q_{m0})\right\} - 1\right]q^{1/3} \qquad \text{(B8)}$$

686 $$\frac{1}{S+1}\frac{dS}{dt} = -A_2 BN^{2/3} S\left(q_{m0} - \frac{1}{A_2}\ln\frac{S+1}{S_{m0}+1}\right)^{1/3} \qquad \text{(B9)}$$

687 Eqs. (B8) and (B9) should be solved with initial conditions $q(0) = q_{m0}$ and $S(0) = S_{m0}$
688 respectively.

689 4. In case $|S_{m0}| << 1$, supersaturation is close to zero all the time $|S(t)| << 1$ and Eqs. (B7-B9)
690 can be simplified as follows

691 $$S(t) = S_{m0} - A_2\left[q(t) - q_{m0}\right] \qquad \text{(B10)}$$

692 $$\frac{dq}{dt} = -BN^{2/3}\left(A_2 q^{4/3} - (A_2 q_{m0} + S_{m0})q^{1/3}\right) \qquad \text{(B11)}$$

693 $$\frac{dS}{dt} = -B(A_2 N)^{2/3}(A_2 q_{m0} + S_{m0} - S)^{1/3} S \qquad \text{(B12)}$$

694

695 5. Then one can obtain Eqs. (B10-B12) in a non-dimensional form. Let us define time scale
696 $\tau_{m0} = \left(BA_2 N^{2/3} q_{m0}^{1/3}\right)^{-1}$, normalized liquid water mixing ratio $\tilde{q} = \frac{q}{q_{m0}}$, normalized supersaturation

697 $\tilde{S} = \frac{S}{A_2 q_{m0}}$, and non-dimensional time $\tilde{t} = t / \tau_{m0} = BA_2 N^{2/3} q_{m0}^{1/3} t$. The Eqs. (B10-B12) can be

698 rewritten in a non-dimensional form as

699 $$\tilde{S}(\tilde{t}) = -\tilde{q}(\tilde{t}) + \gamma \qquad \text{(B13)}$$

700 $$\frac{d\tilde{q}}{d\tilde{t}} = \tilde{q}^{1/3}\left(\gamma - \tilde{q}\right) \qquad \text{(B14)}$$

701 $$\frac{d\tilde{S}}{d\tilde{t}} = -(\gamma - \tilde{S})^{1/3}\tilde{S} \qquad \text{(B15)}$$

702 where non-dimensional parameter $\gamma = 1 + \frac{S_{m0}}{A_2 q_{m0}}$ depends on initial supersaturation S_{m0} and

703 initial liquid water mixing ratio q_{m0}. Eq. (B14) should be solved with initial condition $\tilde{q}(0) = 1$

704 and Eq. (B15) should be solved with initial condition $\tilde{S}(0) = \frac{S_{m0}}{A_2 q_{m0}} < 0$. Note that Eqs. (B14) and

705 (B15) are rigidly connected by Eq. (B13).

706

707 **References**

708 Andejchuk, M., Grabowski, W. W., Malinowski, S. P., and Smolarkiewicz, P. K.: Numerical
709 simulation of cloud–clear air interfacial mixing: homogeneous vs. inhomogeneous mixing., *J.*
710 *Atmos. Sci.*, **66**, 2493–2500, 2009.

711 Anthes, R.A.,: Tropical cyclones-Their evolution, structure, and effects. Monograph 41,
712 Amer. Meteorol. Soc., 208 pp, 1982

713 Baker, M., and J. Latham: The evolution of droplet spectra and the rate of production of
714 embyonic raindrops in small cumulus clouds. *J. Atmos. Sci.*, **36,** 1612–1615, 1979.

715 Baker, M., R. G. Corbin, and J. Latham: The influence of entrainment on the evolution of
716 cloud drop spectra: I. A model of inhomogeneous mixing. *Quart. J. Roy. Meteor. Soc.*, **106,** 581–
717 598, 1980.

718 Baker M. B. and J. Latham: A diffusive model of the turbulent mixing of dry and cloudy air.
719 *Quart. J. R. Met.* Soc., **108**, 871-898, 1982

720 Bar-Or R. Z., I. Koren, O. Altaratz and E. Fredj: Radiative properties of humidified aerosol
721 in cloudy environment. *Atmos. Res.*, **118**, 280–294, 2012.

722 Benmoshe, N., M. Pinsky, A. Pokrovsky, and A. Khain: Turbulent effects on the
723 microphysics and initiation of warm rain in deep convective clouds: 2-D simulations by a
724 spectral mixed-phase microphysics cloud model. *J. Geophys. Res.*, **117**, 1–20, 2012.

725 Benmoshe N., M. Pinsky, A. Pokrovsky and A. Khain: Turbulent effects on microstructure
726 and precipitation of deep convective clouds as seen from simulations with a 2-D spectral
727 microphysics cloud model. *J. Geop. Res*., **117**, D06220, 2012.

728 Blyth, A. M., Choularton, T. W., Fullarton, G., Latham, J., Mill, C. S., Smith, M. H., and
729 Stromberg, I. M.: The Influence of entrainment on the evolution of cloud droplet spectra. 2. Field
730 experiments 5 at Great Dun Fell, *Q. J. Roy. Meteor. Soc*., **106**, 821–840, 1980.

731 Burnet, F., and J-L. Brenguier: Observational study of the entrainment-mixing process in
732 warm convective clouds. *J. Atmos. Sci.*, **64,** 1995–2011, 2007.

733 Denvich B. J., P. Bartello, J-L. Brenguier, L.R. Collins, W.W. Grabowski, R.H.A. Ijzermans,
734 S.P. Malinovski, M.W. Reeks, J.C. Vassilicos, L-P. Wang, and Z. Warhaft: Droplet growth in
735 warm turbulent clouds. *Q. J. Roy. Meteorol. Soc.*, **138**, 1401-1429, 2012.

736 Dimotakis P. E.: Turbulent mixing, *Annu. Rev. Fluid Mech*., **37**, 329-356, 2005.

737 Ferrier, B.S. and R.A. Houze: One-dimensional time dependent modeling of GATE
738 cumulonimbus convection. *J. Atmos. Sci.*, **46**, 330-352, 1989.

739 Gerber H, Frick G, Jensen J.B, and Hudson J.G.: Entrainment, mixing, and microphysics in
740 trade-wind cumulus. *J. Meteorol. Soc. Jpn.*, **86A**. 87-106, 2008.

741 Ghan S. J., Hayder Abdul-Razzak, A. Nenes, Yi Ming, Xiaohong Liu, M. Ovchinnikov, B.
742 Shipway, N. Meskhidze, Jun Xu and X. Shi: Droplet nucleation: Physically-based

743 parameterizations and comparative evaluation, *J. Adv. Model. Earth Syst*., 3, M10001, 33 pp.
744 DOI:10.1029/2011MS000074, 2011.

745 Goix P. J. and L. Talbot: Turbulent counter flow diffusion flame structure and dilution
746 effects combustion. *Science and Technology*, 79, #4-6, 1991.

747 Hill, A. A., G. Feingold, and H. Jiang: The influence of entrainment and mixing assumption
748 on aerosol–cloud interactions in marine stratocumulus. *J. Atmos. Sci.*, 66, 1450–1464, 2009.

749 Jeffery, C. A.: Inhomogeneous cloud evaporation, invariance, and Damköhler number. J.
750 Geophys. Res. 112, D24S21, doi:10.1029/2007JD008789

751 Kerstein A. R.: Linear eddy modelling of turbulent scalar transport and mixing, *Comb. Sci.*
752 *Technol*., 60, 391-421, 1988.

753 Kerstein A. R.: Linear-eddy modelling of turbulent transport. Part 6. Microstructure of
754 diffusive scalar mixing fields. *J. Fluid Mech*., **231**, 361-394, 1991.

755 Khain A., Thara V. Prabha, Nir Benmoshe, G. Pandithurai, M. Ovchinnikov: The mechanism
756 of first raindrops formation in deep convective clouds. *J. Geophys. Res.* Atmospheres**. 118**,
757 9123–9140, 2013.

758 Khain A.P. , K. D. Beheng, A. Heymsfield, A. Korolev, S.O. Krichak, Z. Levin, M. Pinsky,
759 V. Phillips, T. Prabhakaran, A. Teller, S.C. van den Heever, J.-I. Yano: Representation of
760 microphysical processes in cloud-resolving models: spectral (bin) microphysics vs. bulk
761 parameterization. *Review of Geophysics* (in press) , 2015

762 Knight C. A. and L. J. Miller: Early radar echoes from small, warm cumulus: Bragg and
763 hydrometeor scattering. *J. Atmos. Sci.*, **55**, 2974-2992, 1998.

764 Korn G. A. and T. M. Korn: Mathematical handbook for scientists and
765 engineers: Definitions, theorems, and formulas for reference and review. Courier Corporation –
766 Mathematics - 1130 pp, 2000.

767 Korolev, A.V.: The influence of suresaturation fluctuations on droplet size spectra formation.
768 *J. Atmos. Sci.*, **52**, 3620-3634, 1995.

769 Korolev, A. V., and G. A. Isaac: Drop growth due to high supersaturation caused by isobaric
770 mixing. *J. Atmos. Sci.*, **57,** 1675–1685, 2000.

771 Korolev A., V, Isaac, G. A.: Phase transformation of mixed-phase clouds. *Q. J. Roy.*
772 *Meteorol. Soc*. **129**, 19-38, 2003.

773 Korolev, A. V., and I. P. Mazin: Supersaturation of water vapor in clouds. *J. Atmos. Sci.,* **60,**
774 2957–2974, 2003.

775 Korolev A., A. Khain, M. Pinsky, and J. French: Theoretical investigation of mixing in warm
776 clouds. Part 1: Classical concept. Submitted, 2015

777 Kumar B, J. Schumacher, and R. A. Shaw: Cloud microphysical effects of turbulent mixing
778 and entrainment. *Theor. Comput. Fluid Dyn*., **27**, 361–376, 2013.

779 Latham, J. and Reed, R. L.: Laboratory studies of effects of mixing on evolution of cloud
780 droplet spectra, *Q. J. Roy. Meteor. Soc*., **103**, 297–306, 1977.

781 Lehmann, K., H. Siebert, R. A. Shaw: Homogeneous and inhomogeneous mixing in cumulus
782 clouds: Dependence on local turbulence structure. *J. Atmos. Sci.*, **66**, 3641–3659, 2009.

783 Mazin, I. P.: Effect of phase transition on formation of temperature and humidity
784 stratification in clouds. *Proc. Int. Conf. on Cloud Physics.* Toronto, Ontario, Canada, Amer.
785 Meteor. Soc., 132– 137, 1968.

786 Magaritz-Ronen L., M. Pinsky, and A. Khain: Effects of turbulent mixing on the structure
787 and macroscopic properties of stratocumulus clouds demonstrated by a Lagrangian trajectory
788 model. *J. Atmos. Sci.,* **71**, 1843–1862, 2014.

789 Monin, A.S. and Yaglom, A.M.: "Statistical Fluid Mechanics: Mechanics of Turbulence",
790 vol. **2**, MIT Press. 911 pp., 1975.

Pinsky, M. and A. P. Khain: Effects of in-cloud nucleation and turbulence on droplet spectrum formation in cumulus clouds. *Quart. J. Roy. Meteorol. Soc*., **128**, 1–33, 2002.

Pinsky M., I.P. Mazin, A. Korolev, and A. Khain: Supersaturation and diffusional drop growth in liquid clouds, *J. Atmos. Sci.*, **70**, 2778-2793, 2013.

Pinsky M., I. P. Mazin, A. Korolev and A. Khain: Supersaturation and diffusional droplet growth in liquid clouds: Polydisperse spectra. *J. Geophys. Res., Atmospheres,* **119**, 12,872–12,887, 2014

Pruppacher, H.R., Klett, J.D.: Microphysics of clouds and precipitation. 2nd edn. Oxford Press, 914 p. , 1997

De Rooy, W. C., P. Bechtold, K. Fröhlich, C. Hohenegger, H. Jonker, D. Mironov, A. P. Siebesma, J. Teixeira and J-I Yano: Entrainment and detrainment in cumulus convection: an overview, *Q. J. Royal Met. Soc*., **139**, 1–19, 2013.

Stull, Roland B.: An Introduction to Boundary Layer Meteorology. Springer, Netherlands, 666 pp, 1988.

Troen, I. and L. Mahrt: A simple model of the atmospheric boundary layer: Sensitivity to surface evaporation. *Boundary Layer Met.* **37**, 129-148, 1986.

Warhaft Z.: Passive scalars in turbulent flows. *Annu. Rev. Fluid Mech*., **32**, 203–240, 2000.

Warner J.: The microstructure of cumulus cloud. Part 1: general features of the droplet spectrum, *J. Atmos. Sci.*, **26**, 1049-1059, 1969.

812

813 **Table 1.** Linear scales of volumes experiencing homogeneous mixing at conditions typical of

814 different cloud types.

Cloud type	N, cm^{-3}	LWC gm^{-3}	r, μm	Dissipation rate, cm^2/s^3	Phase relaxation time, s	Phase scale, m
Maritime Convective	100	2.0	16.8	300	2.01	0.49
Maritime Stratocumulus	100	0.5	10.6	10	3.19	0.18
Weak Stratocumulus	100	0.2	7.8	5	4.33	0.2
Continental Convective	500	2	8.0	500	0.75	0.6

815

816

817

818 **Table 2.** Estimations of mixing results at different environmental conditions*

T (^{o}C)	A_2	q_1, g/kg	RH_2 %	μ (cloud fraction)	$R\frac{1-\mu}{\mu}$	Result of mixing
$T = 0^oC$	400	1.0	95	0.5	-0.125	cloudy
$T = 0^oC$	400	1.0	50	0.5	-1.25	Non-cloudy
-10^oC	700	2.0	95	0.5	-0.036	cloudy
-10^oC	700	2.0	50	0.5	-0.36	cloudy
-20^oC	1500	2.0	95	0.5	-0.017	cloudy
-20^oC	1500	2.0	50	0.5	-0.17	cloudy
-20^oC	1500	2.0	95	0.1	-0.153	cloudy
-20^oC	1500	2.0	50	0.1	-1.53	Non-cloudy

819 * The values A_2 are estimated as proposed by Pinsky et al., (2013).

820

821

822 **Table 3.** Parameters of the initial Gamma distributions

DSD	N_{m0}, cm^3	α	β, μm	Modal radius, μm	LWC, g/m^3
Narrow	264.2	101.0	0.1	10.0	0.587
Wide	71.0	4.3	3.1	10.0	0.587

823

824

825

826 **Tab. A1. List of symbols**

827

Symbol	Description	Units
A_2	$\frac{1}{q_v}+\frac{L^2}{c_p R_v T^2}$, coefficient	nd
B	$\frac{3}{F}\left(\frac{4\pi\rho_w}{3\rho_a}\right)^{2/3}$, coefficient	$m^2\ s^{-1}$
C	constant of integration	nd
c_p	specific heat capacity of moist air at constant pressure	$J\ kg^{-1}K^{-1}$
$\mathscr{D}$	coefficient of water vapour diffusion in the air	$m^2\ s^{-1}$
e	water vapor pressure	$N\ m^{-2}$
e_S	saturation vapour pressure above a flat water surface	$N\ m^{-2}$
F	$F=\frac{\rho_w L^2}{k_a R_v T^2}+\frac{\rho_w R_v T}{e_S(T)\mathscr{D}}$, coefficient	$m^{-2}\ s$
$f(r,t)$	droplet size distribution	m^{-4}
$f_0(r_0)$	droplet size distribution after the first stage of mixing	m^{-4}
k_a	coefficient of air heat conductivity	$J\ m^{-1}s^{-1}K^{-1}$
L_{mix}	characteristic spatial scale of mixing	m
L_{pr}	spatial scale of phase relaxation	m
L	latent heat for liquid water	$J\ kg^{-1}$
N	droplet concentration	m^{-3}
N_1	droplet concentration in a cloud volume	m^{-3}
N_{m0}	droplet concentration after the first stage of mixing	m^{-3}
p	pressure of moist air	$N\ m^{-2}$
q	liquid water mixing ratio	kg/kg
q_1	liquid water mixing ratio in a cloudy volume	kg/kg
q_{m0}	liquid water mixing ratio after the first stage of mixing	kg/kg
q_w	liquid water content (LWC)	gm^{-3}

q_{w0}	LWC after the first stage of mixing	gm^{-3}
q_v	water vapor mixing ratio	kg/kg
$\tilde{q}$	normalised liquid water mixing ratio equal to normalized LWC	nd
$\tilde{q}_{\min}$	normalized equilibrium liquid water mixing ratio equal to normalized equilibrium LWC	nd
Q	change of square of droplet radius	m^2
r	droplet radius	m
R	$\frac{S_2}{A_2 q_1}$, potential evaporation parameter (PEP)	nd
R_a	specific gas constant of moist air	$J\ kg^{-1}K^{-1}$
R_v	specific gas constant of water vapor	$J\ kg^{-1}K^{-1}$
RH_0	$1+S_{m0}$, relative humidity after the first stage of mixing	nd
S	$e/e_w - 1$, supersaruration over water	nd
S_{m0}	supersaturation after the first stage of mixing	nd
S_2	supersaturation in a dry volume	nd
$\tilde{S}_{\max}$	maximal normalized supersaturation	nd
$\tilde{S}$	normalized supersaturation	nd
T	temperature	K
T_1	temperature in a cloud volume	K
T_2	temperature in a dry volume	K
t_e	normalized evaporation time	nd
t	time	s
$\tilde{t}$	non-dimensional time	nd
$x(\tilde{t})$	non-dimensional variable	nd
α	parameter of the Gamma distribution	nd
β	parameter of the Gamma distribution	m^{-1}
χ	$\gamma^{1/3}$, non-dimensional parameter	nd
ε	turbulent dissipation rate	m^2s^{-3}

γ	$1+\frac{S_{m0}}{A_2 q_{m0}}$, non-dimensional parameter	nd
δq_m	mixing ratio of liquid water required to saturate 1 kg of the cloud (or cloudy?) volume after instant mixing	nd
μ	mass fraction of cloud air	nd
ρ_a	air density	kg m^{-3}
ρ_w	density of liquid water	kg m^{-3}
τ_{pr}	phase relaxation time	s
τ_{mix}	characteristic time of mixing	s
τ_{m0}	time scale	s

"nd" denotes non-dimensional

Figures

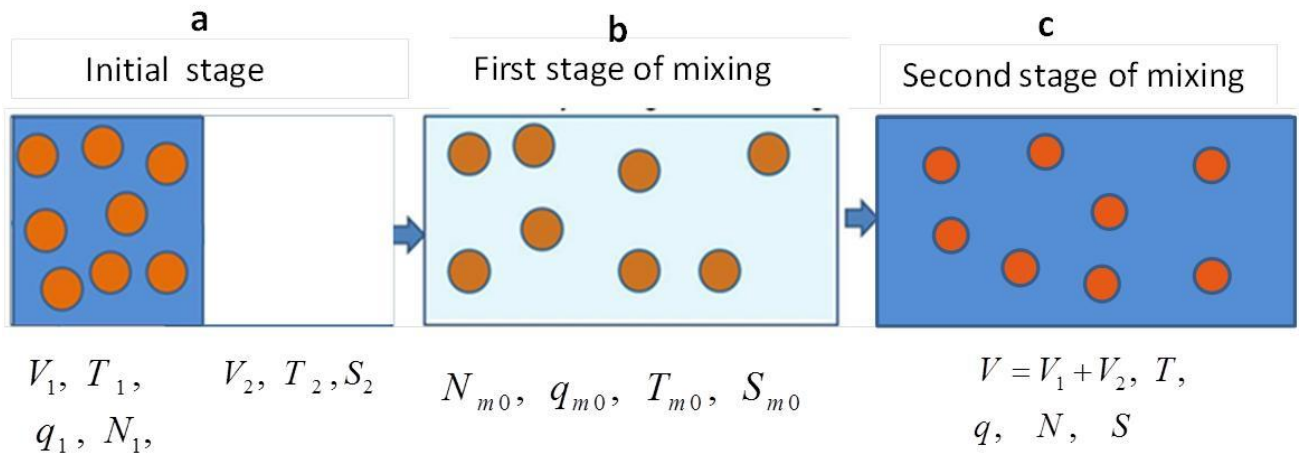

Fig. 1. Conceptual scheme of homogeneous mixing in case of monodisperse DSD. The subsaturated volume of dry air is colored white, and the cloudy volumes with saturated air are colored dark blue. The volume forming as a result of mixing after total homogenization is colored light blue. Index 1 shows the initial values characterizing the initially cloudy volume. Index 2 denotes initial values in the droplet-free volume. Index "$m0$" denotes values in the mixing volume after the first stage of mixing.

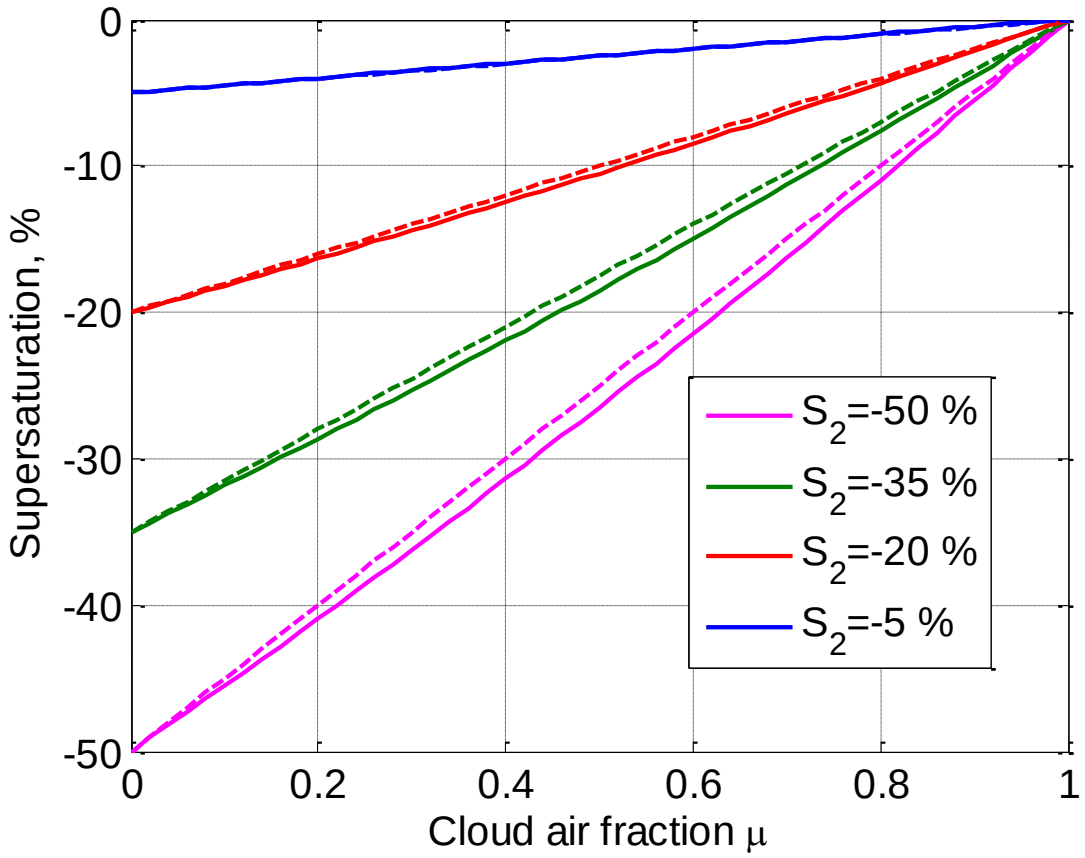

Fig. 2. Dependence of supersaturation on parameter μ: simulation results (solid line) and an approximate linear dependence calculated using Eq. (6b) (dashed line). The initial temperatures of two volumes are $T_1 = 8\,^{o}\mathrm{C}$ and $T_2 = 10\,^{o}\mathrm{C}$.

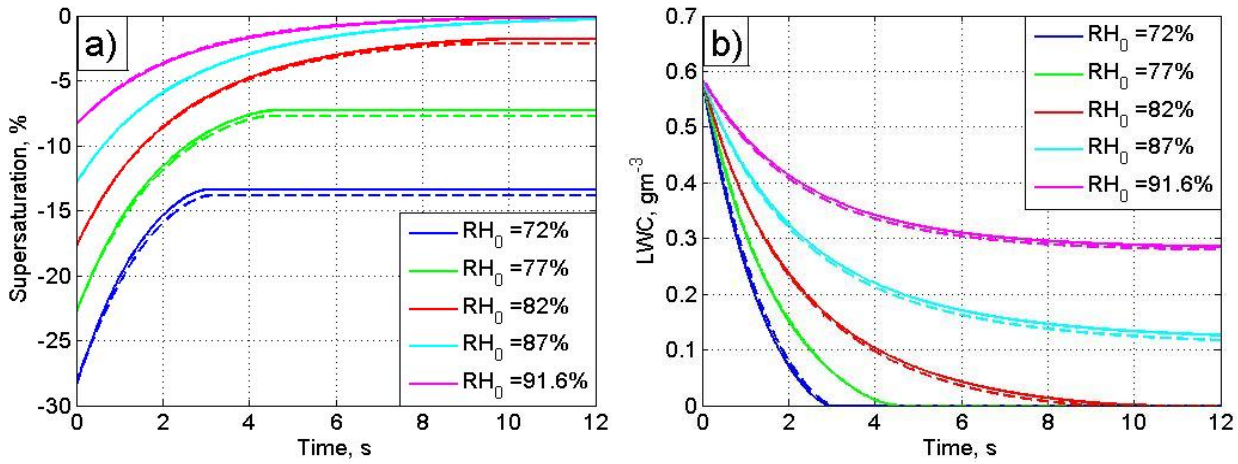

Fig. 3. Dependencies $S(t)$ (a) and $q_w(t)$ (b), calculated at different initial relative humidity RH_0 using closed differential equations (12,13) (solid lines) and using a parcel model (dashed lines). The calculation parameters are $T_{m0} = 10^{o}C$, $p_0 = 842$ mb, $r_0 = 10\ \mu m$, $N_{m0} = 140\ cm^{-3}$, $q_{w0} = 0.58\ gm^{-3}$.

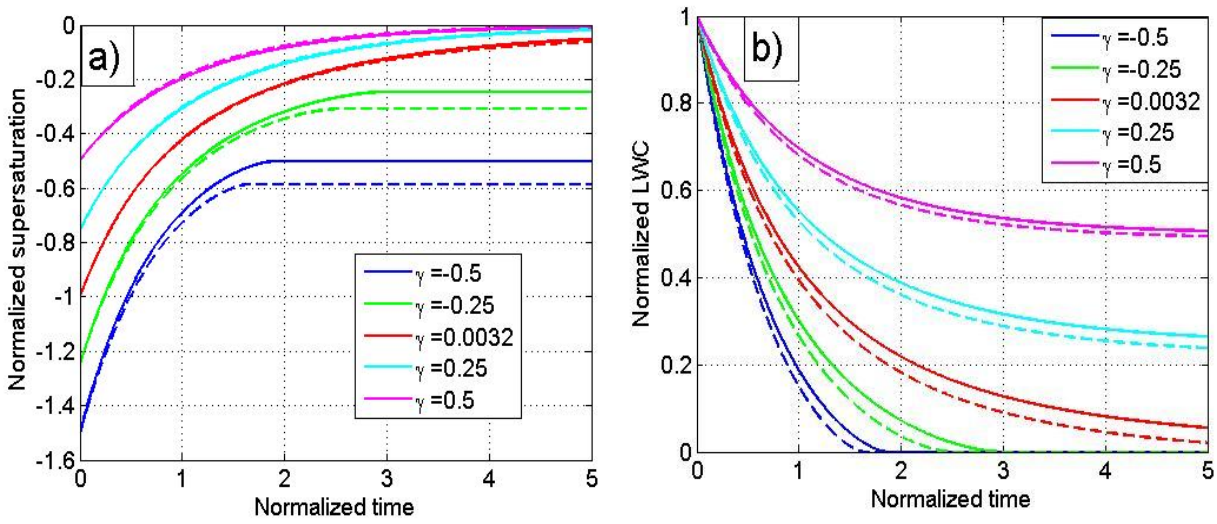

Fig. 4. Universal dependencies $\tilde{S}(\tilde{t})$ (a) and $\tilde{q}(\tilde{t})$ (b), calculated at different values of parameter γ using Eqs. (17-18) (solid lines) and using a parcel model (dashed lines).

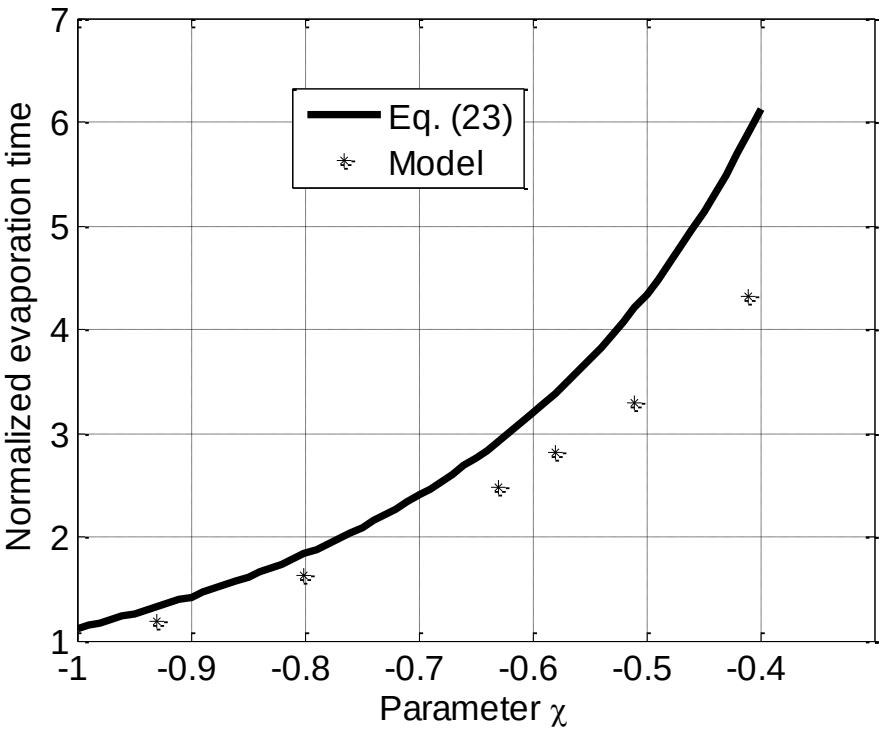

Fig. 5. Dependence of the evaporation time on parameter χ, $t_e(\chi)$. Time is measured at the relaxation time scales. The values obtained using a parcel model are shown by asterisks.

968

969

970

971

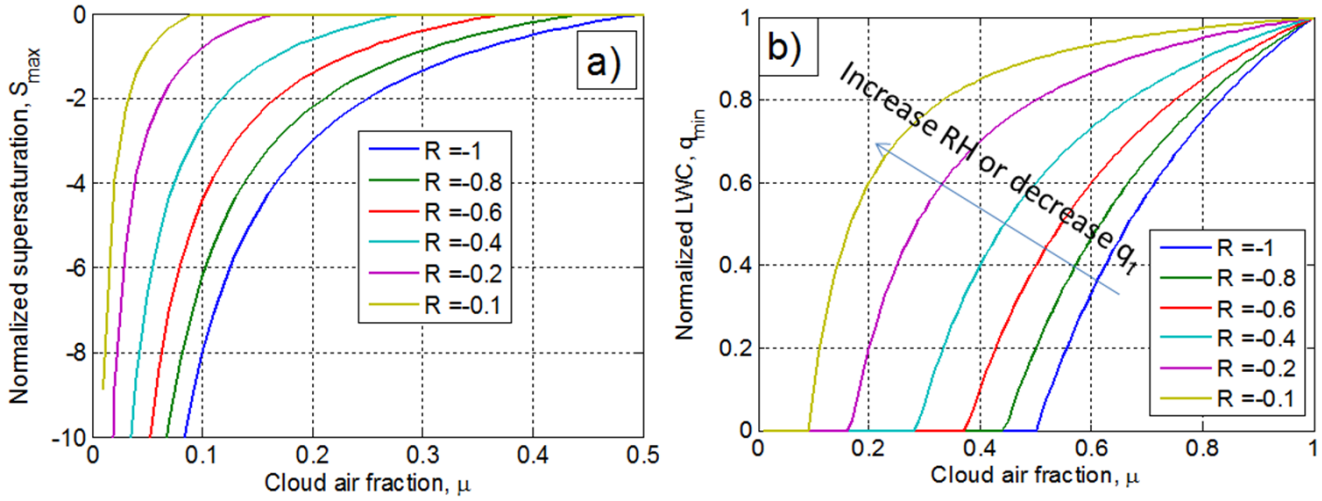

972

973

974 **Fig. 6.** Dependencies of normalized equilibrium supersaturation $\tilde{S}_{max}$ (a) and normalized

975 equilibrium LWC (which is equal to normalized equilibrium liquid water mixing ratio) $\tilde{S}_{max}$ (b)

976 on cloudy air fraction at the final stage of homogeneous mixing. Curves of different colors

977 correspond to different values of non-dimensional parameter $R = \frac{S_2}{A_2 q_1}$.

978

979

980

981

982

983

984

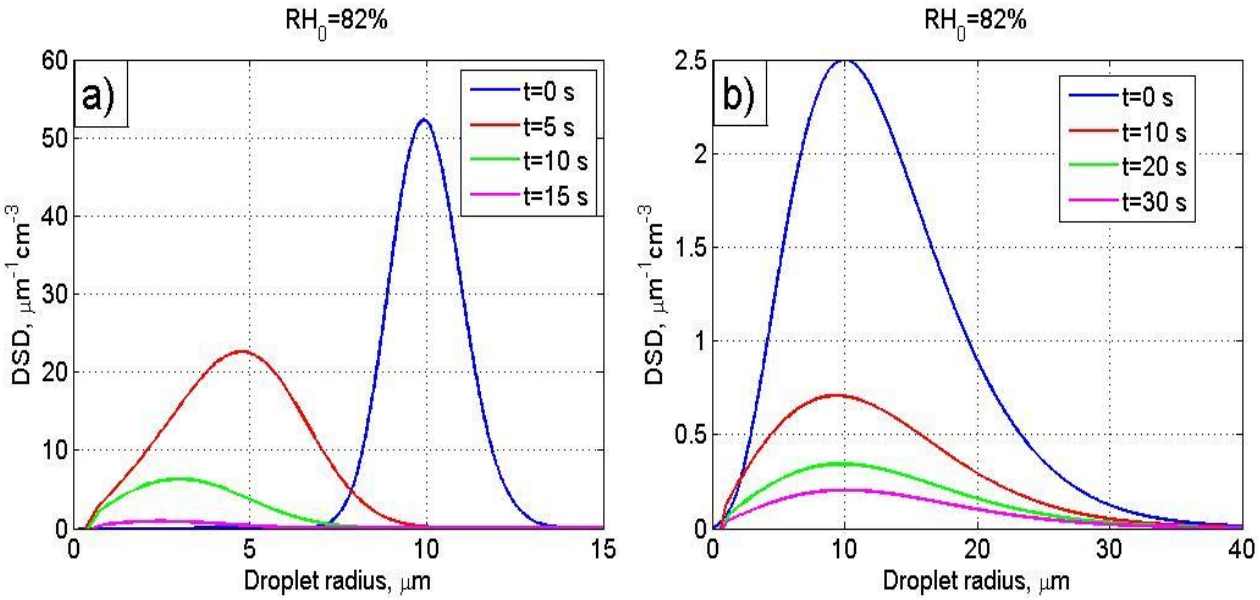

Fig. 7. Time evolution of an initially narrow DSD (a) and an initially wide DSD (b). The initial calculation parameters are the same in both examples: $T_{m0} = 10\ ^{o}C$, $p = 829$ mb, $RH_{m0} = 82\ \%$ and $q_{w0} = 0.587$ g/m^3. The parameters of the initial Gamma distributions are given in Tab. 3.

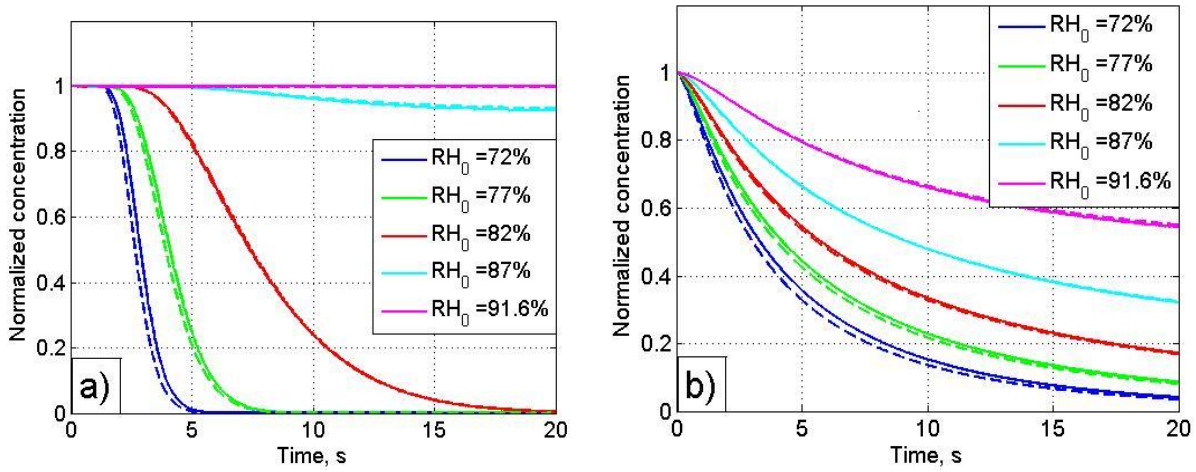

Fig.8. Time dependencies of normalized droplet concentration for an initially narrow DSD (a) and an initially wide DSD (b) at initially different values of RH_0 in the resulting volume. The dependencies are calculated directly using a parcel model (solid lines) and using Eq. (33) (dashed lines). The thermodynamic parameters are the same as in Fig.7. Parameters of the initial DSDs are given in Tab. 3.

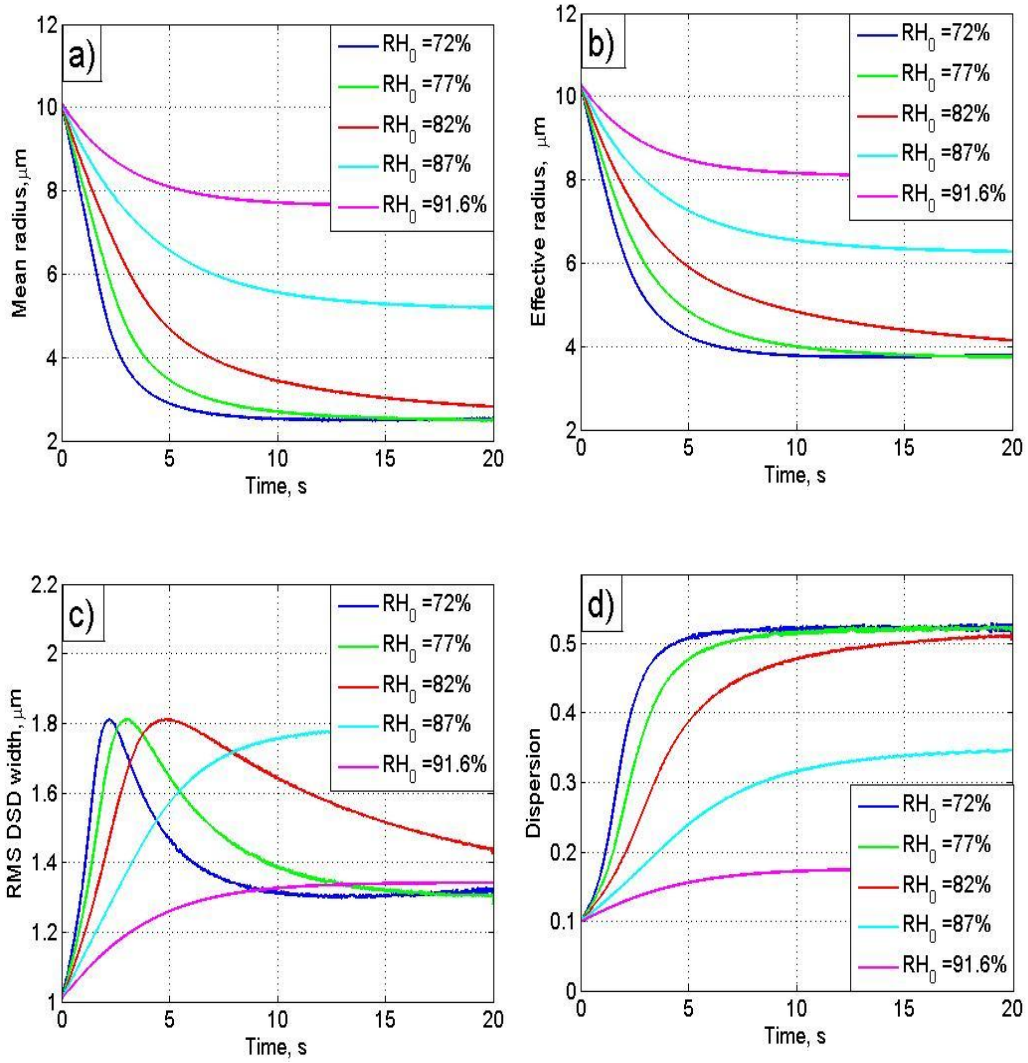

Fig. 9. Dependencies of moment functions typically used for characterizing DSD shape at different values of the initial relative humidity RH_0 in the resulting volume. The dependencies are calculated using a parcel model for an initially narrow DSD (Tab. 3). The thermodynamic parameters are the same as in Fig. 7.

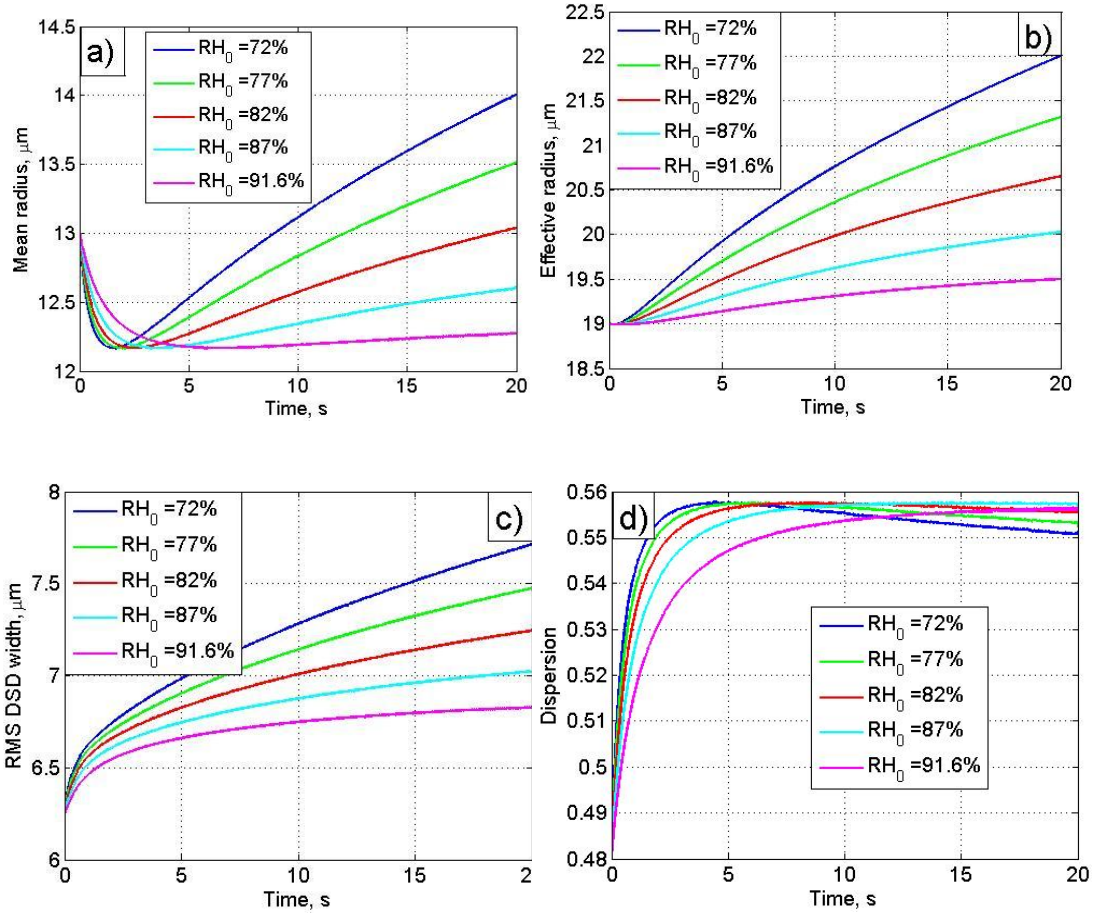

Fig. 10. The same as in Fig. 9 but for an initially wide DSD.

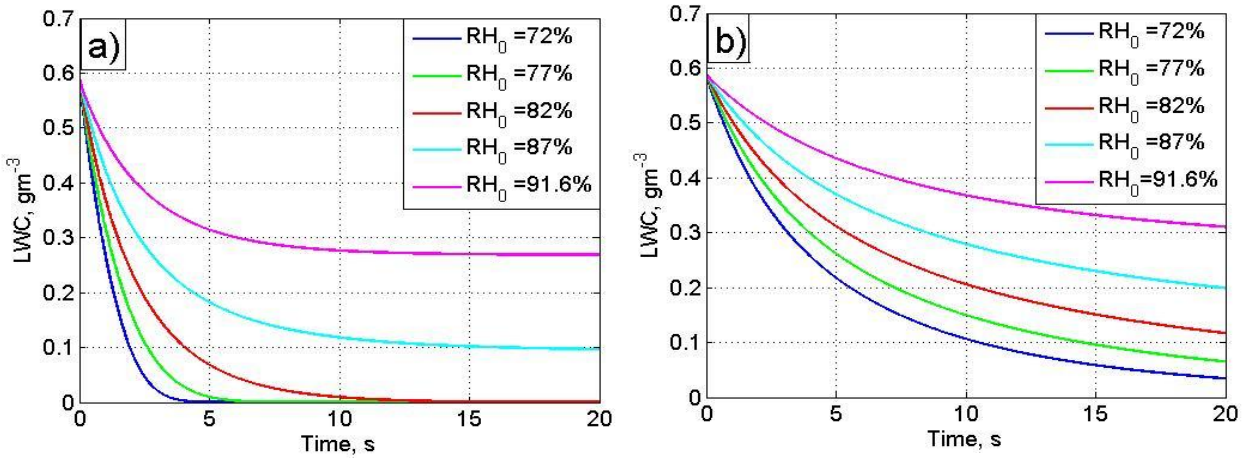

Fig. 11. Time dependencies of LWC calculated using a parcel model at different values of RH_0 in the resulting volume, for an initially narrow DSD (a) and an initially wide DSD (b). The thermodynamic parameters are the same as in Fig.7. The parameters of the initial DSDs are given in Tab. 3.

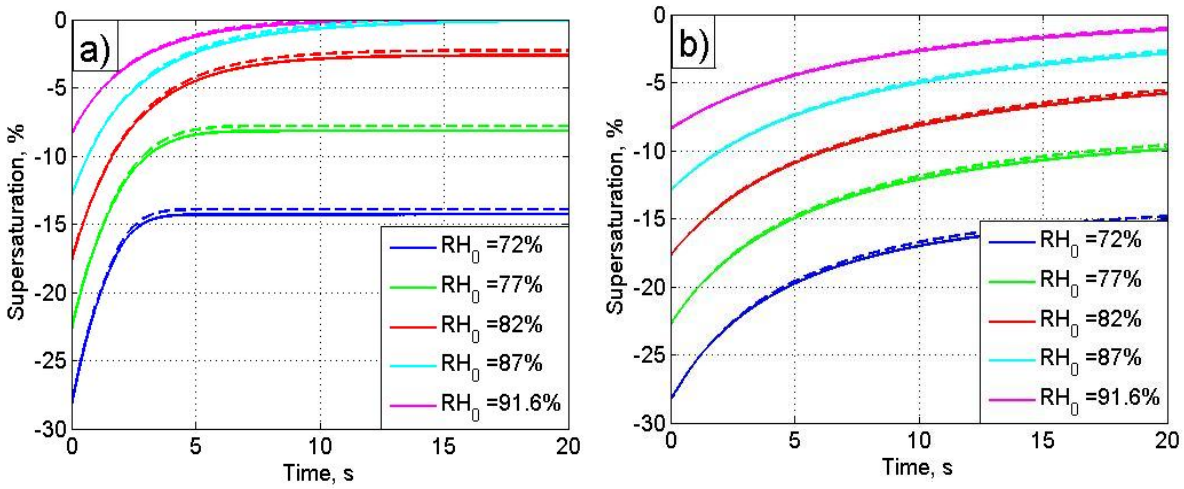

Fig. 12. Time dependencies of supersaturation calculated at different values of the initial relative humidity RH_0 in the resulting volume, using Eq. (8) (solid lines) and Eq. (40) (dashed lines), for an initially narrow DSD (a) and an initially wide DSD (b). The thermodynamic parameters are the same as in Fig.7. The parameters of the initial DSDs are given in Tab.3.

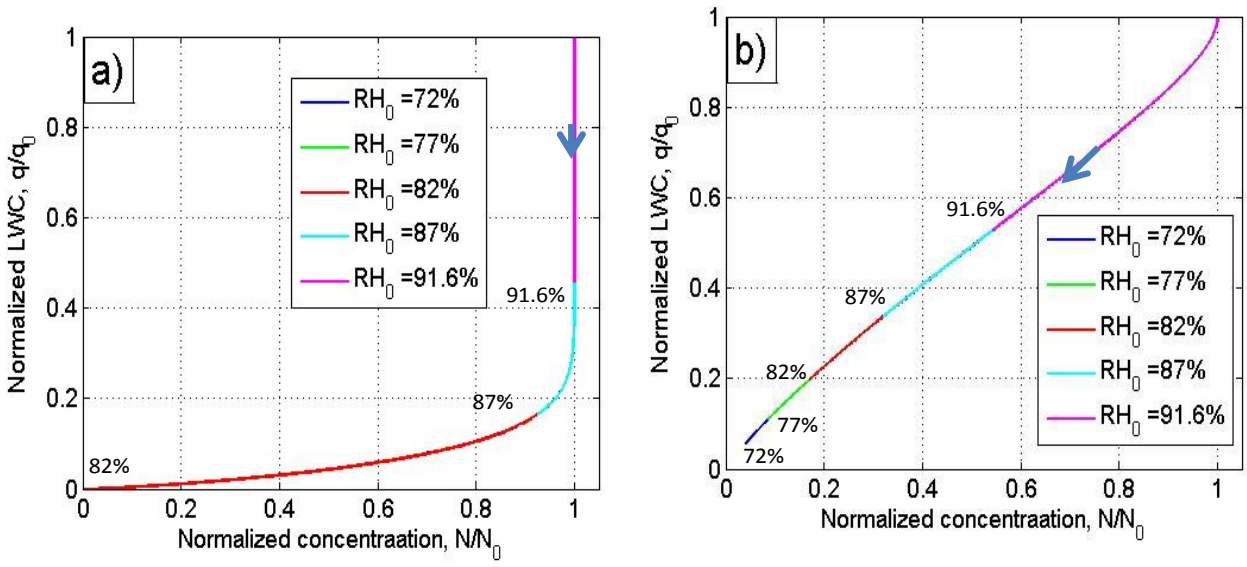

Fig. 13. Dependencies of normalized LWC on the normalized number concentration of droplets calculated at different values of the initial relative humidity RH_{m0} in the resulting volume, for an initially narrow DSD (a) and an initially wide DSD (b). The thermodynamic parameters are the same as in Fig.7. The parameters of the initial DSDs are given in Tab. 3. Arrows denote the direction of increasing time.